International Journal of the Physical Sciences Vol. 6(24), pp. 5623-5647, 16 October, 2011
Available online at http://www.academicjournals.org/IJPS
DOI: 10.5897/IJPS10.571
ISSN 1992 - 1950 ©2011 Academic Journals

Full Length Research Paper

Effectiveness of 3D geoelectrical resistivity imaging using parallel 2D profiles

A. P. Aizebeokhai[1]*, A. I. Olayinka[2], V. S. Singh[3] and C. C. Uhuegbu[1]

[1]Department of Physics, Covenant University, Ota, Nigeria.
[2]Department of Geology, University of Ibadan, Ibadan, Nigeria.
[3]National Geophysical Research Institute, Hyderabad, India.

Accepted 18 April, 2011

Acquisition geometry for 3D geoelectrical resistivity imaging in which apparent resistivity data of a set of parallel 2D profiles are collated to 3D data set was evaluated. A set of parallel 2D apparent resistivity data were generated over two model structures. The models, horst and trough structures, simulates the geological environment of a weathered profile and refuse dump site in a crystalline basement complex, respectively. The apparent resistivity data were generated for Wenner-alpha (WA), Wenner-beta (WB), Wenner-Schlumberger (WSC), dipole-dipole (DDP), pole-dipole (PDP), and pole-pole (PP) arrays with minimum electrode separations (a = 2, 4, 5 and 10 m) and inter-line spacing (L = a, 2a, 2.5a, 4a, 5a and 10a). The 2D apparent resistivity data for each of the arrays were collated to 3D data set and inverted using a full 3D inversion code. The 3D imaging capability and resolution of the arrays for the set of parallel 2D profiles are presented. Grid orientation effects, which decrease with decreasing inter-line spacing, are observed in the inversion images. Inter-line spacing of not greater than four times the minimum electrode separation gives reasonable inverse models. The resolution of the inverse models can be greatly improved if the 3D data set is built by collating sets of orthogonal 2D profiles.

Key words: Acquisition geometry, parallel 2D profiles, 3D surveys, geoelectrical resistivity, 3D imaging, inversion.

INTRODUCTION

The use of 2D/3D geoelectrical resistivity imaging to address a wide variety of hydrological, environmental and geotechnical issues is increasingly popular. The subsurface geology in environmental and engineering investigations is often subtly heterogeneous and multi-scale such that both lateral and vertical variations of the subsurface properties can be very rapid and erratic. The use of vertical electrical sounding is grossly inadequate to map such complex and multi-scale geology. Two-dimensional (2D) geoelectrical resistivity imaging, in which the subsurface is assumed to vary vertically down and laterally along the profile but constant in the perpendicular direction, has been used to investigate areas with moderately complex geology (Griffiths and Barker, 1993; Dahlin and Loke, 1998; Olayinka and Yaramanci, 1999; Amidu and Olayinka, 2006; Aizebeokhai et al., 2010). But subsurface features are inherently three-dimensional and the 2D assumption is commonly violated for such heterogeneous subsurface. This violation often leads to out-of plane resistivity anomaly in the 2D inverse models which could be misleading in the interpretation of subsurface features (Bentley and Gharibi, 2004; Gharibi and Bentley, 2005). Thus, a three-dimensional (3D) geoelectrical resistivity imaging which allows resistivity variation in all possible directions should give more accurate and reliable inverse resistivity models of the subsurface, especially in highly heterogeneous cases.

The composition of a 3D data set that would yield significant 3D subsurface information is less understood. Ideally, a complete 3D data set of apparent resistivity should be made in all possible directions. The techniques for conducting 3D electrical resistivity surveys have been presented by Loke and Barker (1996a). The use of pole-pole (Li and Oldenburg, 1994; Loke and Barker, 1996a; Park, 1998) and pole-dipole (Chambers et al., 1999; Ogilvy et al., 1999) arrays have been reported. Square and rectangular grids of electrodes with constant

*Corresponding author. E-mail: aaizebeokhai@covenant university.com.

electrode spacing in both x- and y-directions, in which each electrode is in turn used as current electrode and the potential measured at all other electrode positions, were commonly used. But these methods which allow the measurements of complete 3D data sets are usually impractical due to the length of cables, the number of electrodes and the site geometry involved in most practical surveys. Also, the measurement of complete 3D data sets using the square or rectangular grids of electrodes is time consuming and cumbersome in surveys involving large grids. This is because the number of possible electrode permutations for the measurements will be very large.

To reduce the number of data measurements as well as the time and effort required for 3D geoelectrical resistivity field surveys, a cross-diagonal surveying technique in which apparent resistivity measurements are made only at the electrodes along the x-axis, y-axis and 45° diagonal lines was proposed by Loke and Barker (1996a). The cross-diagonal surveying method also involves very large number of independent measurements for medium to large grids of electrodes. Hence, the measurement of 3D data set using cross-diagonal technique is time consuming, especially if a single channel or a manual data acquisition system is employed. The inversion of these large volumes of data is often problematic because the computer memory may not be sufficient for the data inversion. In contrasts to the cross-diagonal surveying method, set of orthogonal 2D lines (Bentley and Gharibi, 2004; Gharibi and Bentley, 2005; Aizebeokhai et al., 2009; 2010) which allow flexible survey design, choice of array and easy adaptability to data acquisition systems have been used for 3D geoelectrical resistivity imaging.

In this paper, Wenner-alpha (WA), Wenner-beta (WB), Wenner-Schlumberger (WSC), dipole-dipole (DDP), pole-dipole (PDP) and pole-pole (PP) arrays were used to generate apparent resistivity data in a set of parallel 2D profiles over two synthetic models, horst and trough models. The synthetic models simulate the geological conditions of a weathered profile and refuse dump site in a crystalline basement complex, respectively, which are often associated with geophysical applications for hydro-geological, environmental and engineering investigations. The calculated apparent resistivity data of the parallel set of 2D profiles over the models were collated to 3D data sets for each array investigated and processed using a full 3D inversion code (Loke and Barker, 1996b; Loke and Dahlin, 2002). The imaging capabilities of the parallel set of 2D profiles for 3D surveys were evaluated. The responses of these model structures to 3D inversion for the different arrays were assessed using the 3D inverse models. Differences in the arrays spatial resolution, tendency to produce near surface artefacts in the 3D inverse models and the deviation from true resistivity models as well as the optimum spacing between the parallel set of 2D lines(inter-line spacing) relative to the minimum electrode separation required to form 3D data sets that would yield significant information in 3D inverse models are evaluated.

METHODS OF STUDY

Description of the synthetic models

In this study, two model geometries, host and trough models that represent the geological conditions of a typical weathered profile and refuse dump site in a crystalline basement complex in tropical areas, were designed. These geological conditions are often associated with geophysical applications to hydrogeological, environmental and engineering investigations. The horst structure with a finite lateral extent (Figure 1(a) varies laterally in thickness such that the horst thickens towards the centre where the least weathering is thought to occur and is thinning outward with increasing weathering activities. The horst structure consists of a three-layer model comprising of the top soil, saprolite (the weathered zone) and the fresh basement. The top layer, corresponding to the top soil, was assigned a uniform thickness of 2.5 m and its resistivity varies laterally between 500, 700 Ωm and in the 400 Ωm west-east direction. Varying lateral degrees of weathering or fracturing that increases outward is assigned to the weathered zone (middle layer) with thickness ranging from a minimum of 5.75 m (depth 8.25 m) at the centre of the model structure where the least weathering occurs to a maximum of 13.50 m (depth 16.0 m) at the edges of the model considered to be most weathered. The weathered zone in crystalline basement complex is a product of chemical weathering which is usually a low resistive saprolite overlying a more resistive basement rocks (Carruthers and Smith, 1992; Hazell et al., 1992) and the zone is commonly aquiferous, thus low values of resistivity ranging from a minimum of 150 Ωm to a maximum of 100 Ωm were assigned. Underlying the weathered zone is a fresh basement of infinite thickness with a constant model resistivity of 3000 Ωm. Horizontal depth slices of the actual model resistivities are given in Figure 2.

Similarly, the trough structure of finite lateral extent (Figure 1b) consists of a three-layer model in which the thicknesses of the top and the middle layers varies to a maximum of 4.2 and 11.8 m, respectively, and the underlying layer is a basement rock of infinite thickness. The trough structure varies laterally in thickness and cuts across the first and second layers. Model resistivity of 300 and 600 Ωm were assigned to the first and second layers in their natural states. The trough structure and its surroundings are thought to be impacted by the deposited waste in the simulated dump site and hence would consist of laterally varying low model resistivity. Model resistivity varying laterally between 50 and 250 Ωm different from the assigned values of 300 and 600 Ωm in its natural state, were therefore assigned respectively to the trough structure. Part of the second layer underlying the trough structure is also thought to be impacted by leachates from the deposited waste so that its model resistivity varies to a minimum of 400 Ωm from the assigned value of 600 Ωm in its natural state. A constant model resistivity of 2500 Ωm was assigned to the underlying basement of infinite thickness since the leachates from the deposited waste thought not to have reach the basement. Horizontal depth slices of the actual model resistivities are presented in Figure 3.

Apparent resistivity pseudosections

The model structures were approximated into series of parallel 2D model structures separated with a constant interval. Apparent resistivity data were computed over the set of 2D profiles using the finite difference method (Dey and Morrison, 1979; Loke and Barker, 1996b,) for the following arrays: Wenner-alpha (WA), Wenner-beta (WB), Wenner-Schlumberger (WSC), dipole-dipole (DDP), pole-

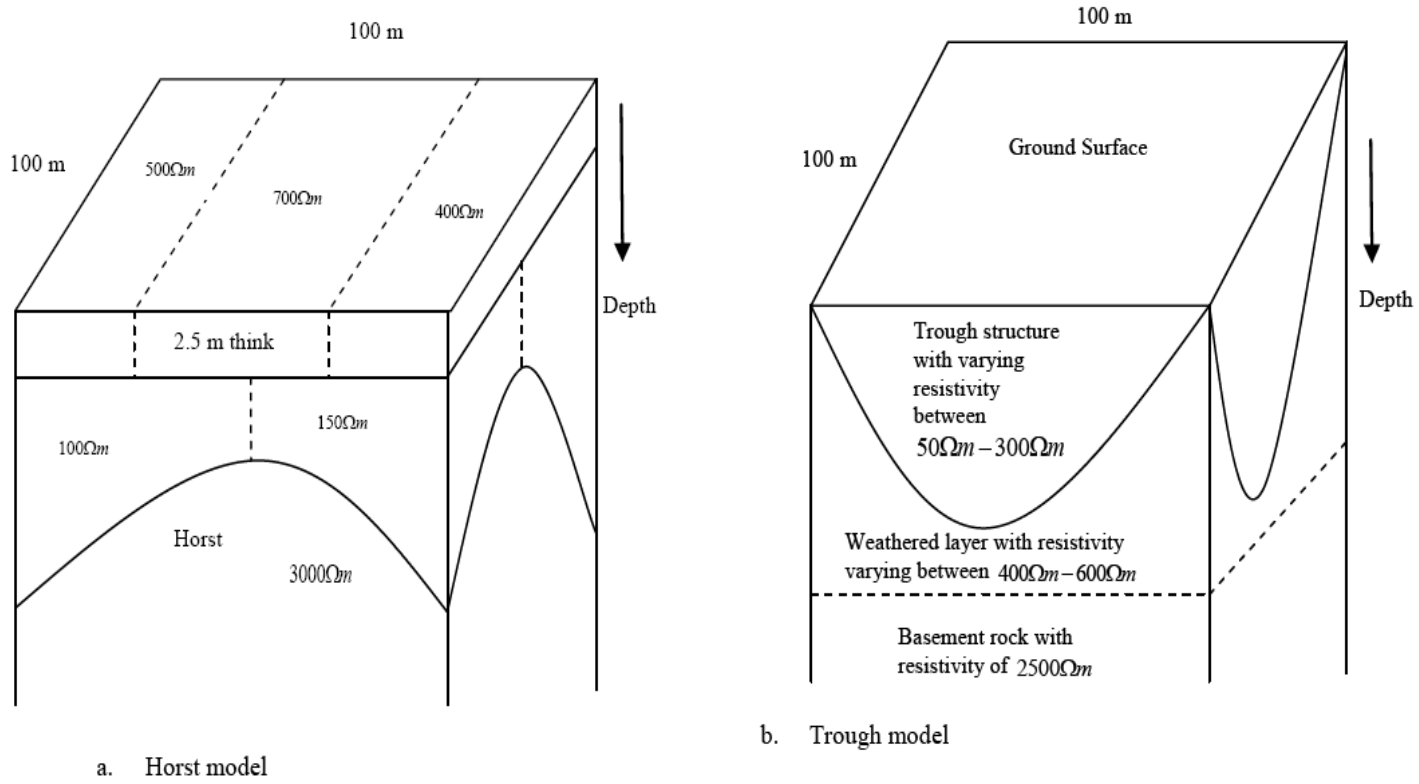

Figure 1. Synthetic models: (a) horst model simulating a typical weathered or fractured profile developed above crystalline basement complex, and (b) trough model simulating the geology of a waste dump site.

dipole (PDP) and pole-pole (PP) arrays. Electrode layouts with minimum separations, a (a = 2 m, 4 m, 5 m and 10 m) and inter-line spacing, L (L = a, 2a, 2.5a, 4a, 5a and 10a) were used in the computation of the apparent resistivity data.

The 2D models were subdivided into a number of homogeneous and isotropic blocks using a rectangular mesh. The resistivity of each of the model was allowed to vary arbitrarily along the profile and with depth, but with an infinite perpendicular extension. The finite difference method basically determines the potentials at the nodes of the rectangular mesh. The apparent resistivity values were normalised with the values of a homogeneous earth model so as to reduce the errors in the computed potential values. The forward modelling grid used consists of four nodes per unit electrode. 5% Gaussian noise (Press et al., 1996) was added to the computed apparent resistivity data for each 2D profile so as to simulate field conditions.

Data collation and inversion

The apparent resistivity data computed for the set of parallel 2D profiles were collated to 3D data set. The collations arranged the apparent resistivity data and the electrode layouts in square grids according the coordinates and direction of each 2D profile used, and electrodes positions in the profiles. Thus, the size and pattern of the electrode grid depends on the number of electrodes in each 2D profile and number of profiles collated. The collated 3D data sets were inverted using a 3D resistivity inversion code (Loke and Barker, 1996b; Loke and Dahlin, 2002) which automatically determines a 3D inverse model of resistivity distribution using apparent resistivity data obtained from a 3D resistivity survey (Li and Oldenburg, 1994; White et al., 2001).

Ideally, the electrodes used for such surveys are arranged in squares or rectangular grids. Smoothness constrained inversion method was employed in inverting the data sets. The mesh sizes for the 3D inversion are based on the grid sizes of the collated data sets. However, the mesh sizes are much less than those for the corresponding 3D data sets that would be collated from orthogonal 2D profiles or those of the conventional square or rectangular 3D surveys. The inversions were carried out to investigate the resolution power of the 3D survey using parallel 2D lines and the effects of different line spacing. The inversion routine used is based on the implementation of the smoothness constrained least-squares method (de Groot-Hedlin and Constable, 1990; Sasaki, 1992).

RESULTS

The 3D inverse model resistivity obtained for electrode grid sizes of 21 × 6 with inter-line spacing of $4a$, a being the minimum electrode separation, are presented as representatives of the inversion models. Horizontal depth slices of the 3D inverse model resistivity of the horst model structure for the selected arrays are given in Figures 4 to 6. Actual model resistivities of the horst structure are given in Figure 2. The sensitivity models of the inverse models presented in Figures 4 to 6 are given in Figures 10 to 12. Similarly, the inversion models obtained for electrode grid sizes of 26 × 6 with inter-line spacing of $5a$, are presented as representatives of the inverse models for the trough structures. Horizontal depth

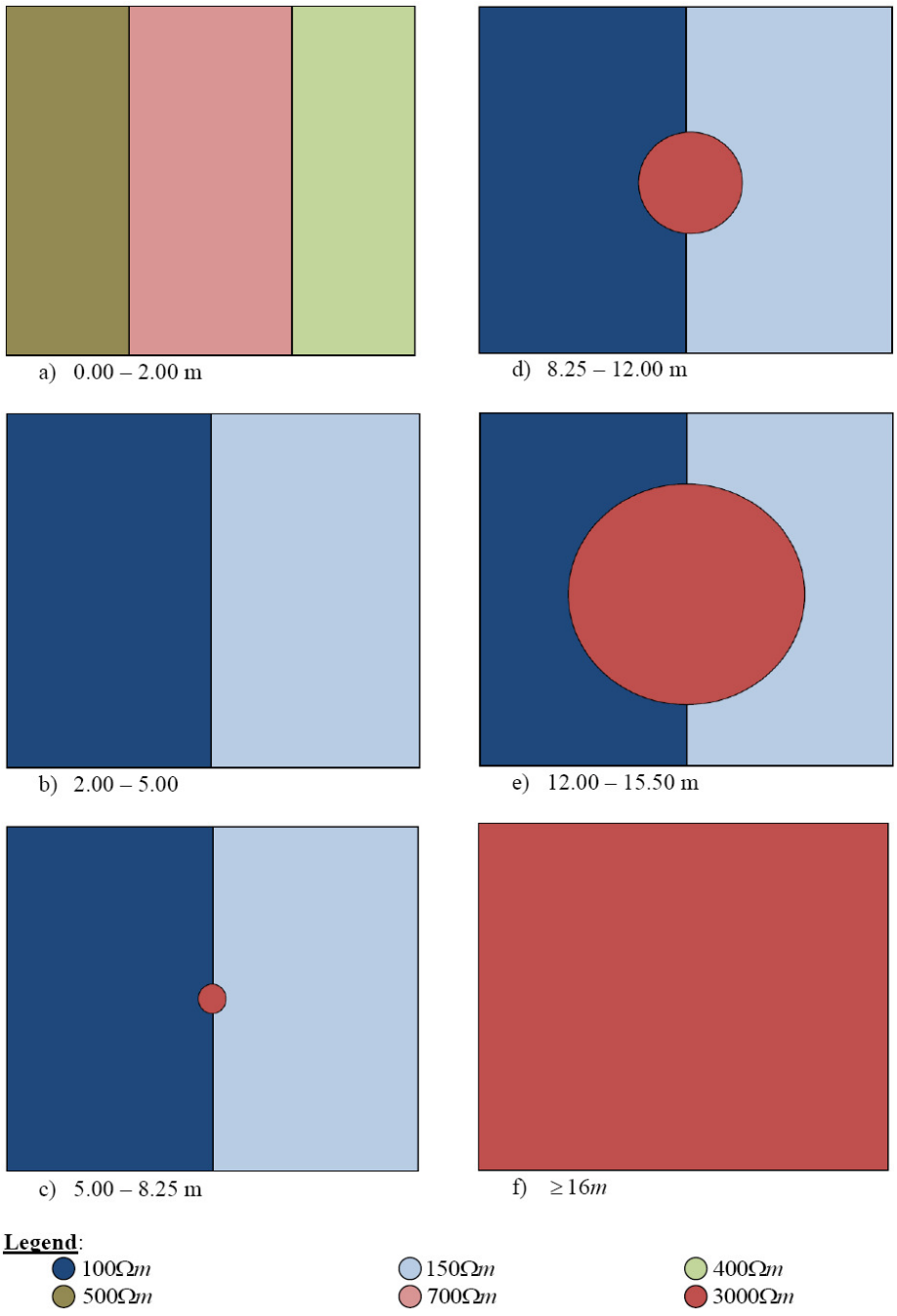

Figure 2. Horizontal depth slices of actual model resistivities for the horst structure.

slices of the 3D inverse model resistivity for the selected arrays are given in Figures 7 to 9. Actual model resistivity values of the trough structure are given in Figure 3.The corresponding sensitivity models for the various electrode arrays are given in Figures 13 to 15.

DISCUSSION

The use of parallel 2D profiles in 3D geoelectrical resistivity imaging provides a fast and cost effective tool for site characterization, and can be used in subsurface investigations for environmental and engineering applications. A comparison of the images obtained from the 3D inversion of the parallel 2D profiles (horizontal depth slices present in Figures 4 to 6 and Figures 7 to 9) to the actual model resistivities (Figures 1 and 2) show that 3D imaging using parallel 2D profiles is relatively efficient. The resolution of the 3D inversion images increases with decreasing inter-line spacing between the

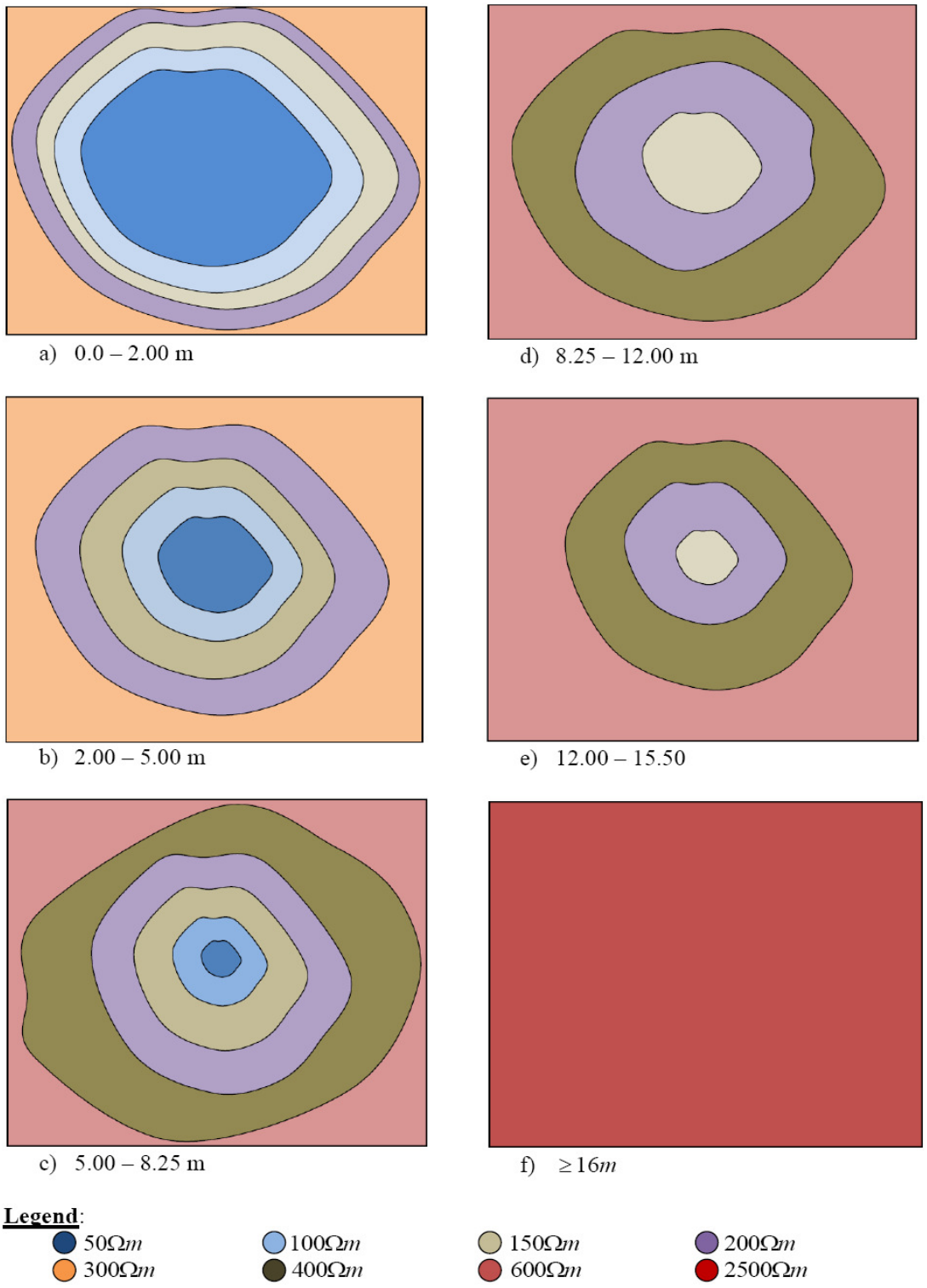

Figure 3. Horizontal depth slices of actual model resistivities for the trough structure.

2D profiles. Inter-line spacing of the order of four times the minimum electrode separation would yield inversion images with acceptable resolution (Garibi and Bentley, 2005; Aizebeokhai et al., 2010). The resolution of the 3D inverse models can be greatly improved if orthogonal set of 2D profiles are used. The inter-line spacing need not be the same in both directions; and the time and resources available for the survey should, to a large extend, determine the inter-line spacing to be used relative to the minimum electrode separation in both directions.

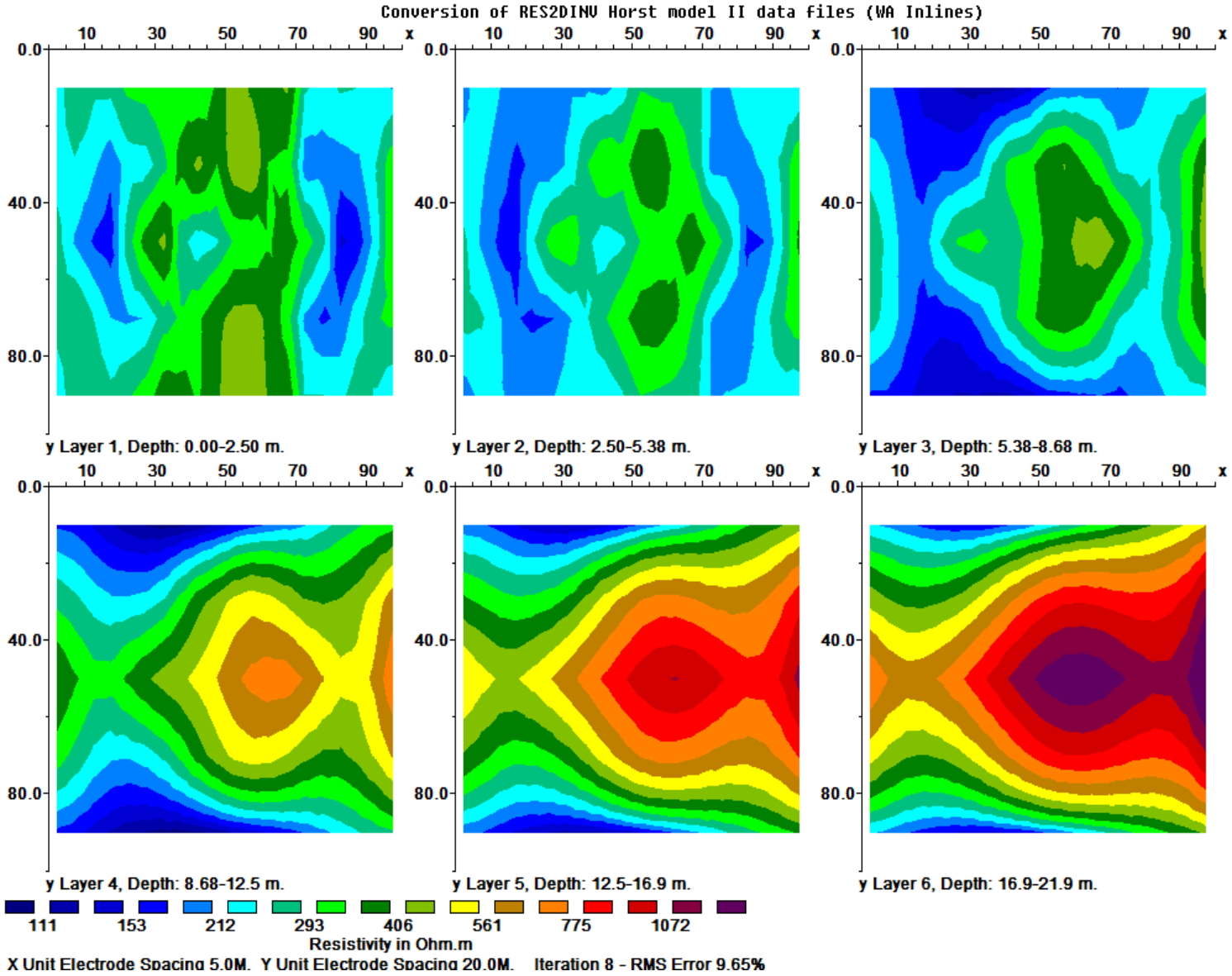
Conversion of RES2DINV Horst model II data files (WA Inlines)
10 30 50 70 90 x
0.0
40.0
80.0
y Layer 1, Depth: 0.00-2.50 m.
y Layer 2, Depth: 2.50-5.38 m.
y Layer 3, Depth: 5.38-8.68 m.
y Layer 4, Depth: 8.68-12.5 m.
y Layer 5, Depth: 12.5-16.9 m.
y Layer 6, Depth: 16.9-21.9 m.
111 153 212 293 406 561 775 1072
Resistivity in Ohm.m
X Unit Electrode Spacing 5.0M. Y Unit Electrode Spacing 20.0M. Iteration 8 - RMS Error 9.65%

(a)WA

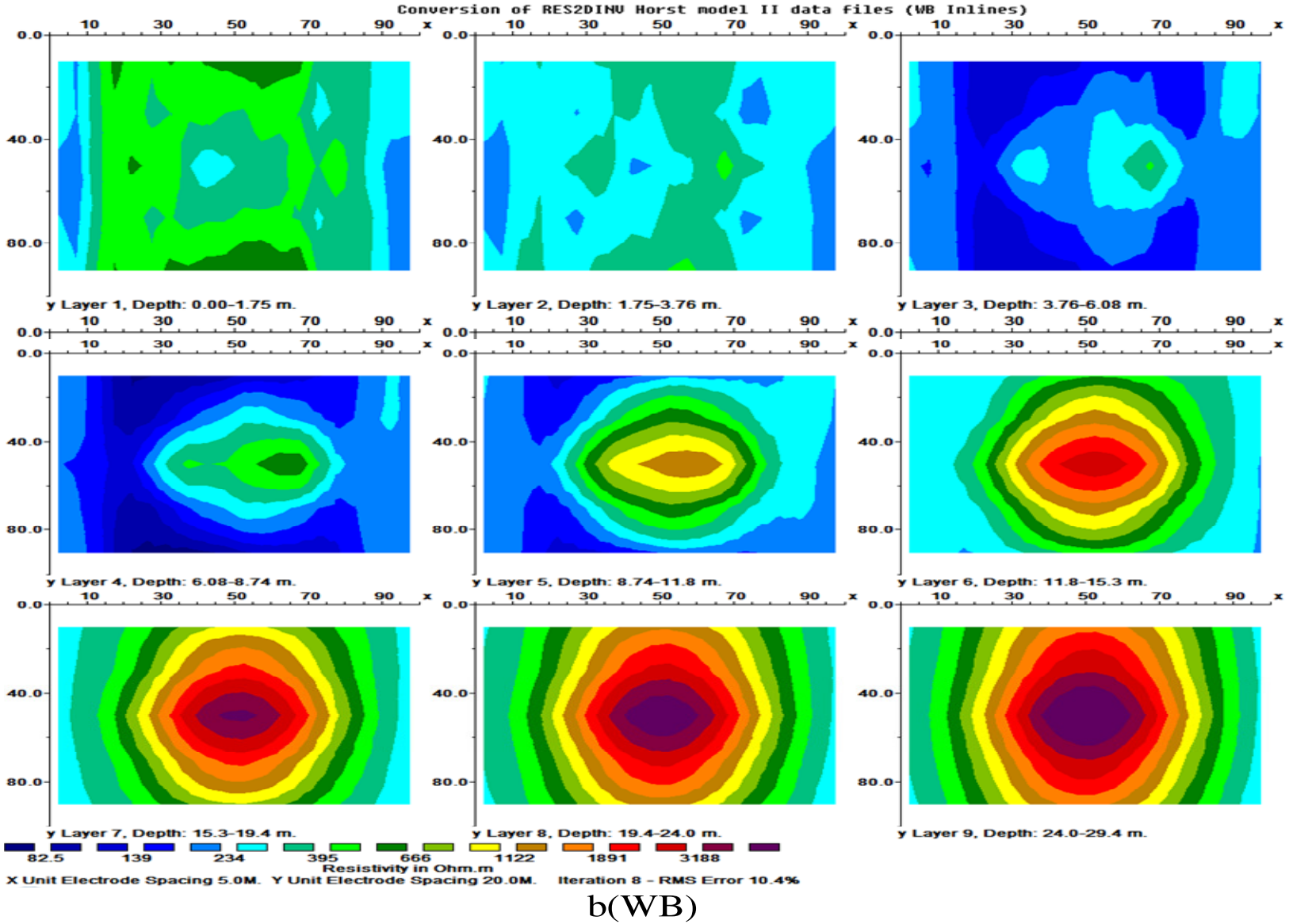

Figure 4. Horizontal depth slices of the inverse models of parallel 2D profiles for the horst model structure with a grid size of 21x6 and inter-line spacing of $4a$: (a) Wenner-alpha; and (b) Wenner-beta.

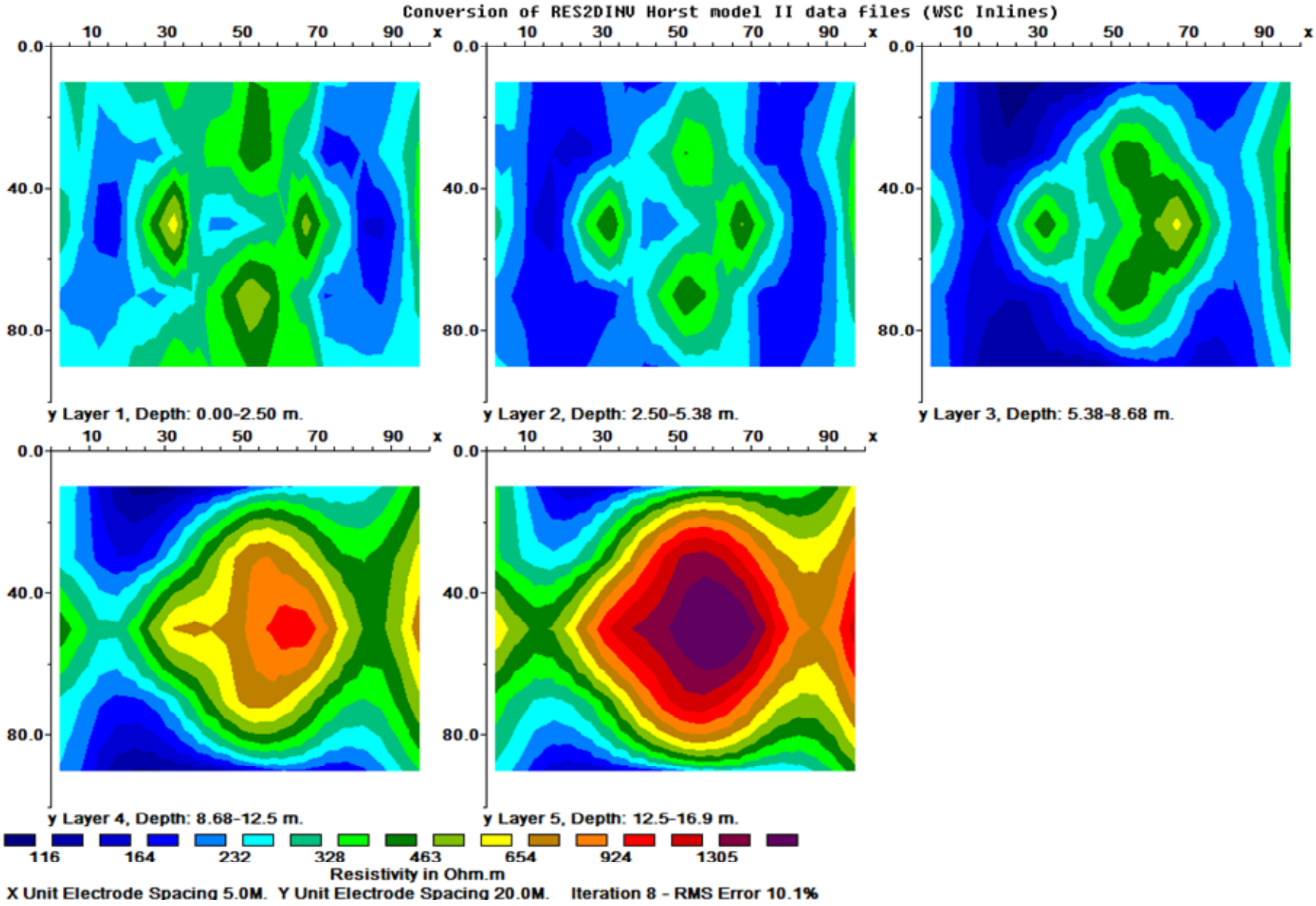
Conversion of RES2DINV Horst model II data files (WSC Inlines)
10 30 50 70 90 x
0.0
40.0
80.0
y Layer 1, Depth: 0.00-2.50 m.
y Layer 2, Depth: 2.50-5.38 m.
y Layer 3, Depth: 5.38-8.68 m.
y Layer 4, Depth: 8.68-12.5 m.
y Layer 5, Depth: 12.5-16.9 m.
116 164 232 328 463 654 924 1305
Resistivity in Ohm.m
X Unit Electrode Spacing 5.0M. Y Unit Electrode Spacing 20.0M. Iteration 8 - RMS Error 10.1%

a(WSC)

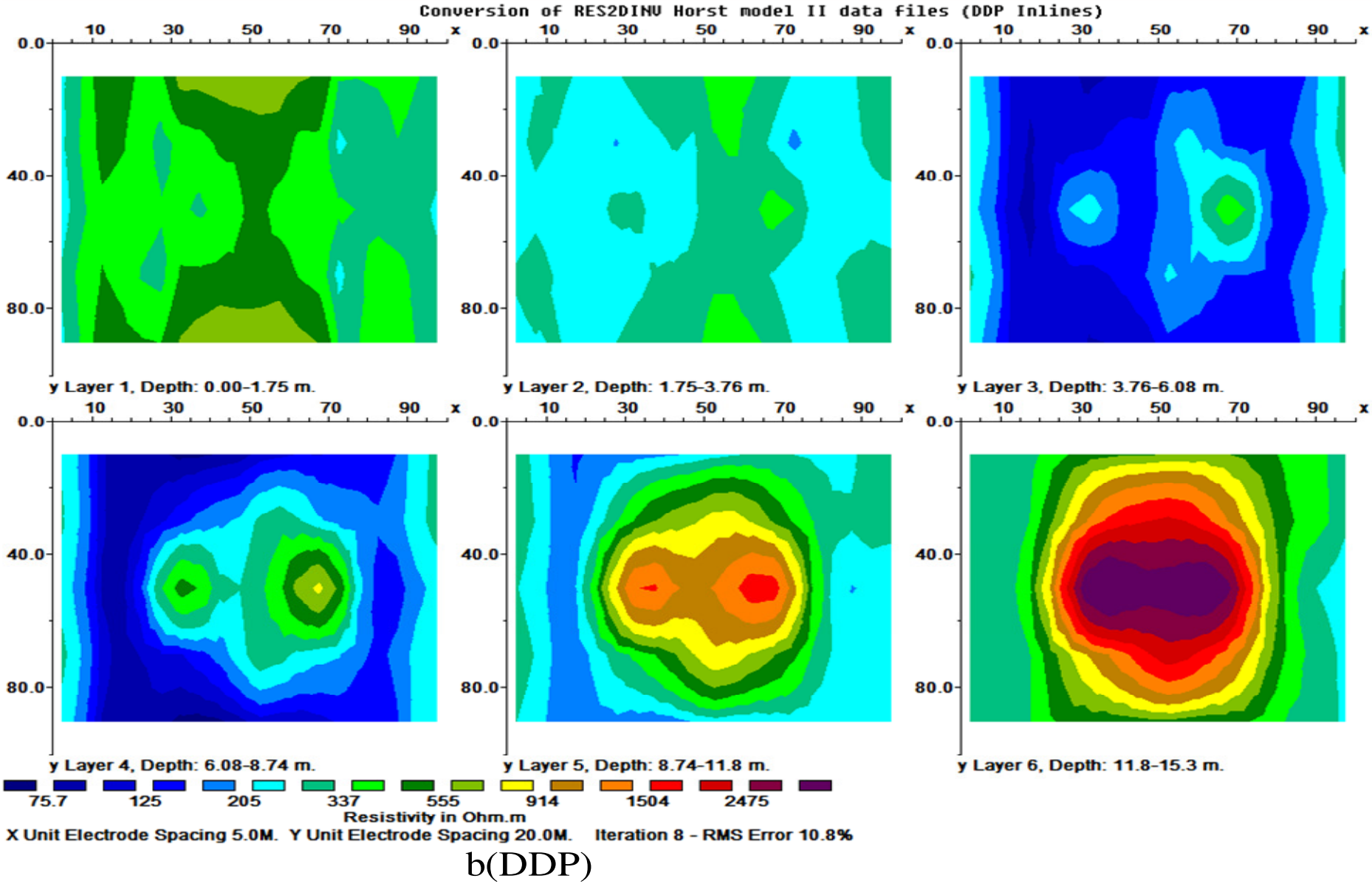

Figure 5. Horizontal depth slices of inverse models of parallel 2D profiles for horst model structure with a grid size of 21×6 and inter-line spacing of $4a$: (a) Wenner-Schlumberger; and (b) dipole-dipole arrays.

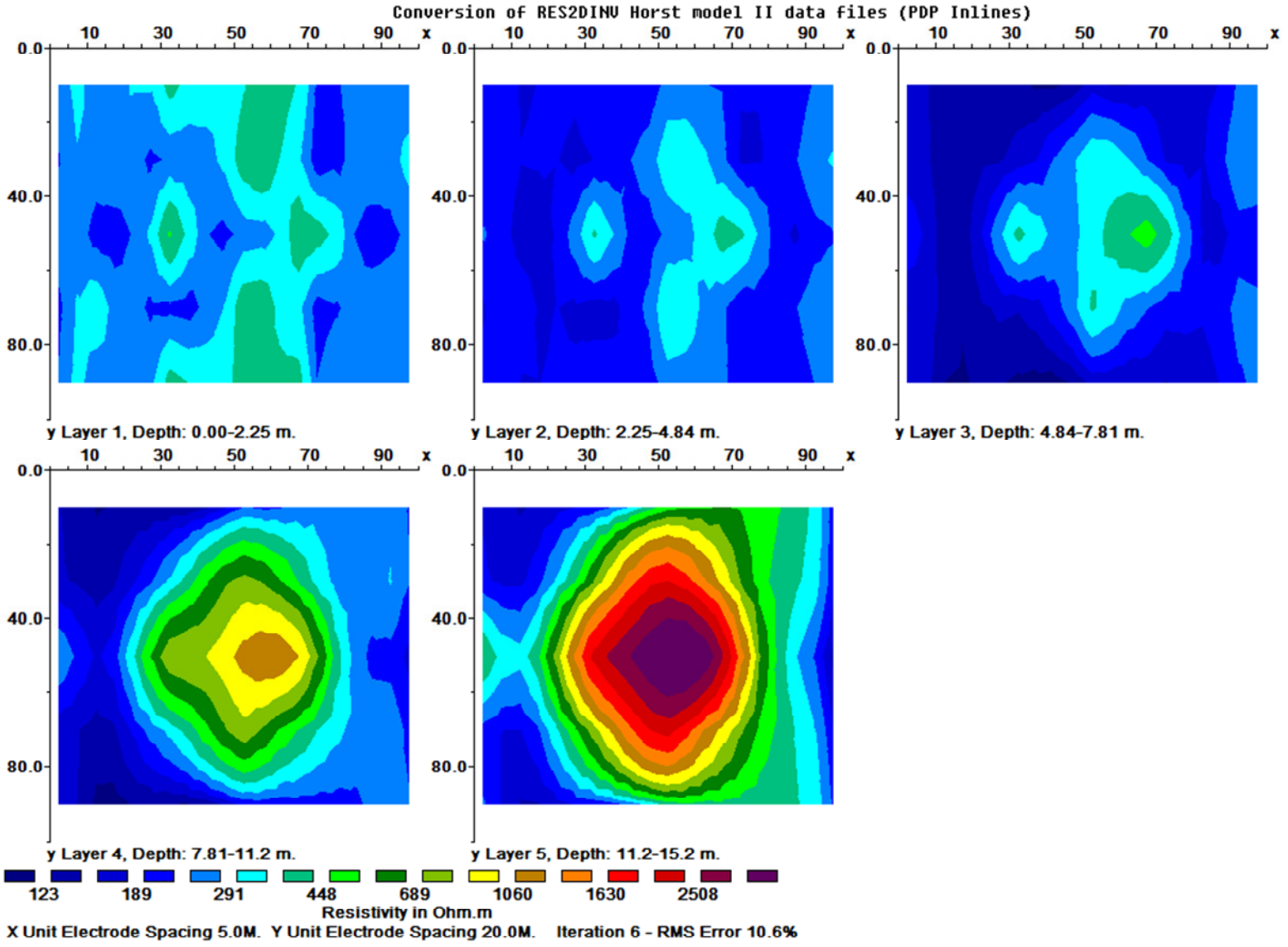
Conversion of RES2DINV Horst model II data files (PDP Inlines)
10 30 50 70 90 x
0.0
40.0
80.0
y Layer 1, Depth: 0.00-2.25 m.
y Layer 2, Depth: 2.25-4.84 m.
y Layer 3, Depth: 4.84-7.81 m.
y Layer 4, Depth: 7.81-11.2 m.
y Layer 5, Depth: 11.2-15.2 m.
123 189 291 448 689 1060 1630 2508
Resistivity in Ohm.m
X Unit Electrode Spacing 5.0M. Y Unit Electrode Spacing 20.0M. Iteration 6 - RMS Error 10.6%

a(PDP)

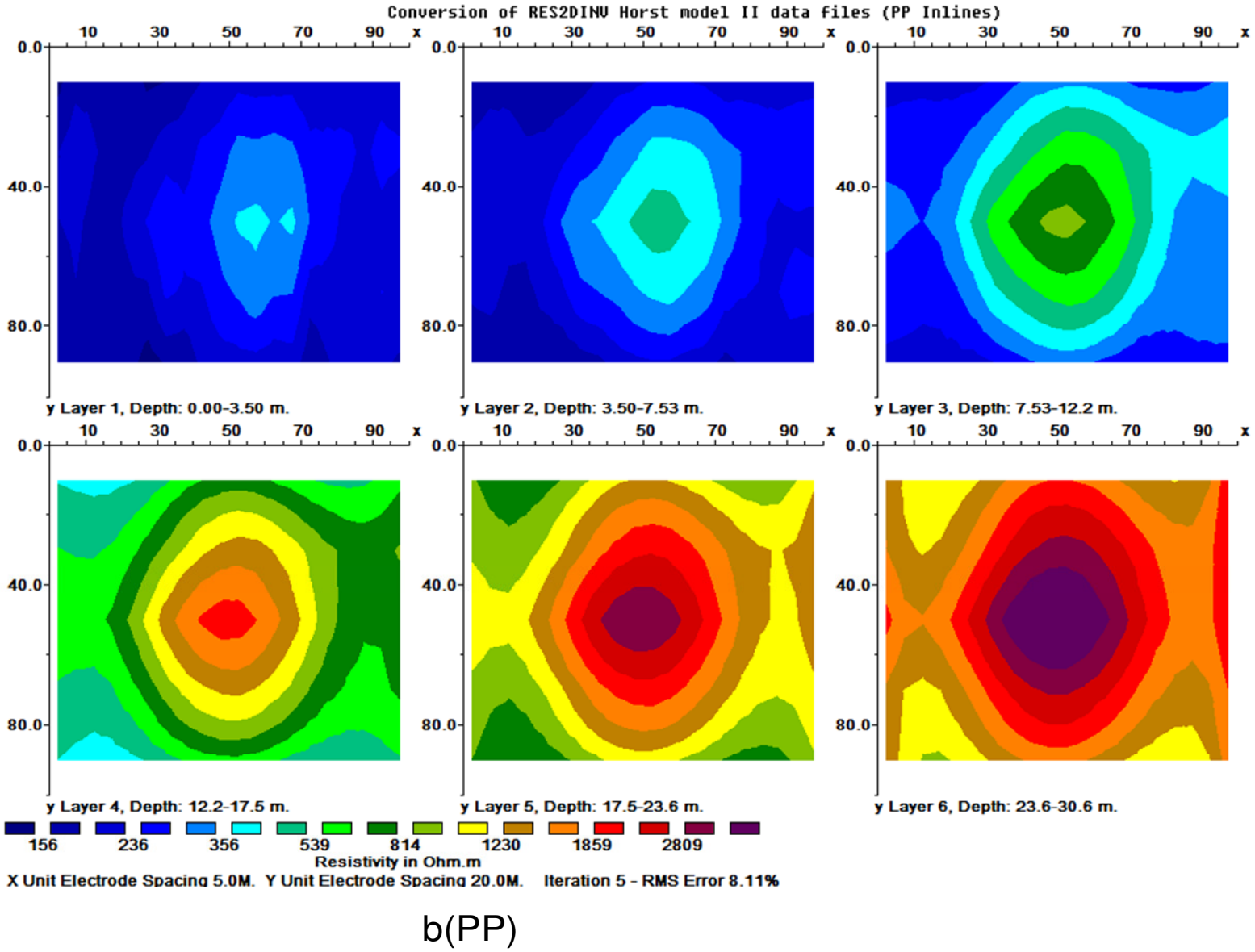

Figure 6. Horizontal depth slices of inverse models of parallel 2D profiles for horst model structure with a grid size of 21×6 and inter-line spacing of $4a$: (a) pole-dipole; (b) pole-pole arrays.

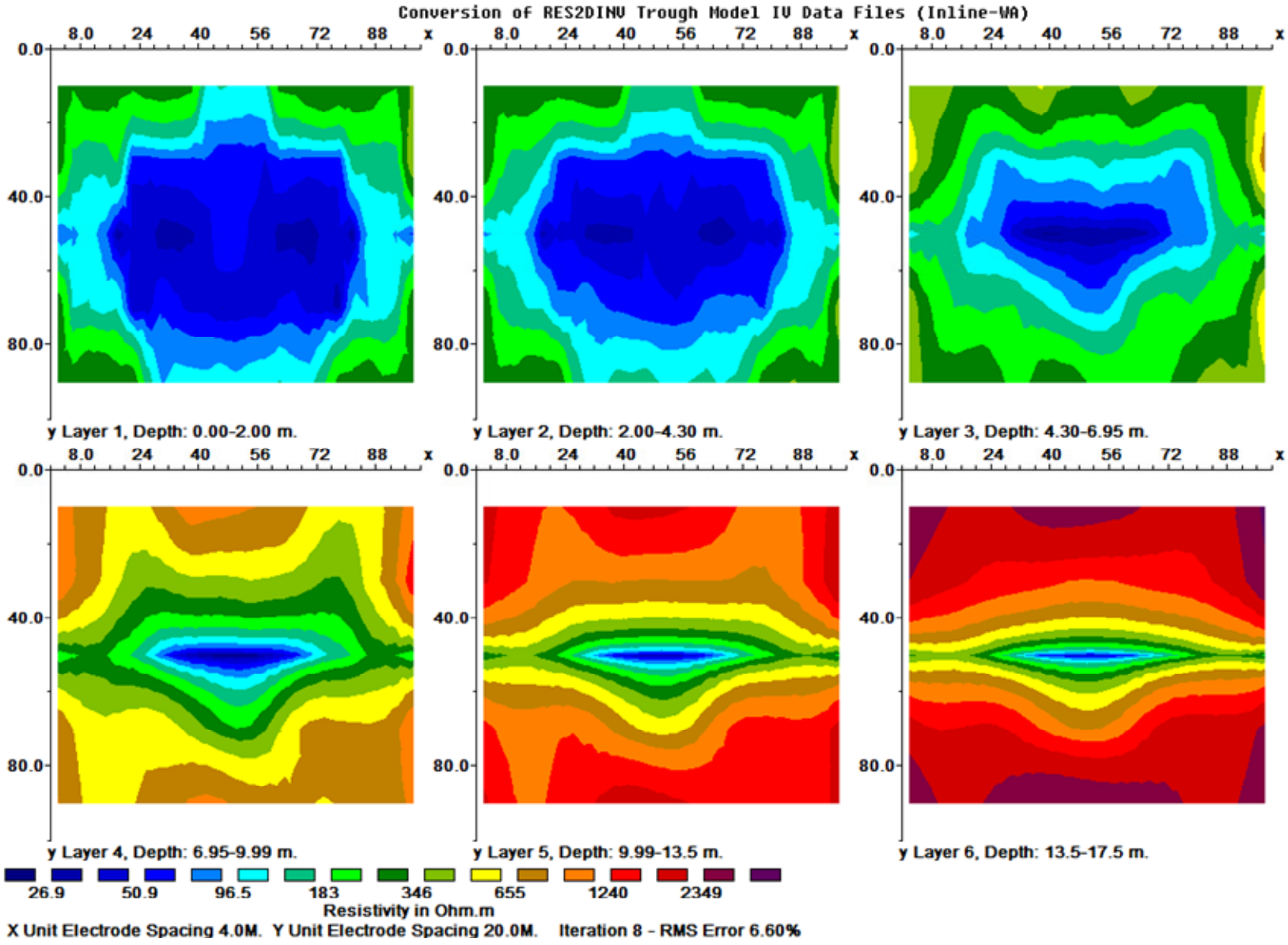
Conversion of RES2DINV Trough Model IV Data Files (Inline-WA)
8.0 24 40 56 72 88 x
0.0
40.0
80.0
y Layer 1, Depth: 0.00-2.00 m.
y Layer 2, Depth: 2.00-4.30 m.
y Layer 3, Depth: 4.30-6.95 m.
y Layer 4, Depth: 6.95-9.99 m.
y Layer 5, Depth: 9.99-13.5 m.
y Layer 6, Depth: 13.5-17.5 m.
26.9 50.9 96.5 183 346 655 1240 2349
Resistivity in Ohm.m
X Unit Electrode Spacing 4.0M. Y Unit Electrode Spacing 20.0M. Iteration 8 - RMS Error 6.60%

a (WA)

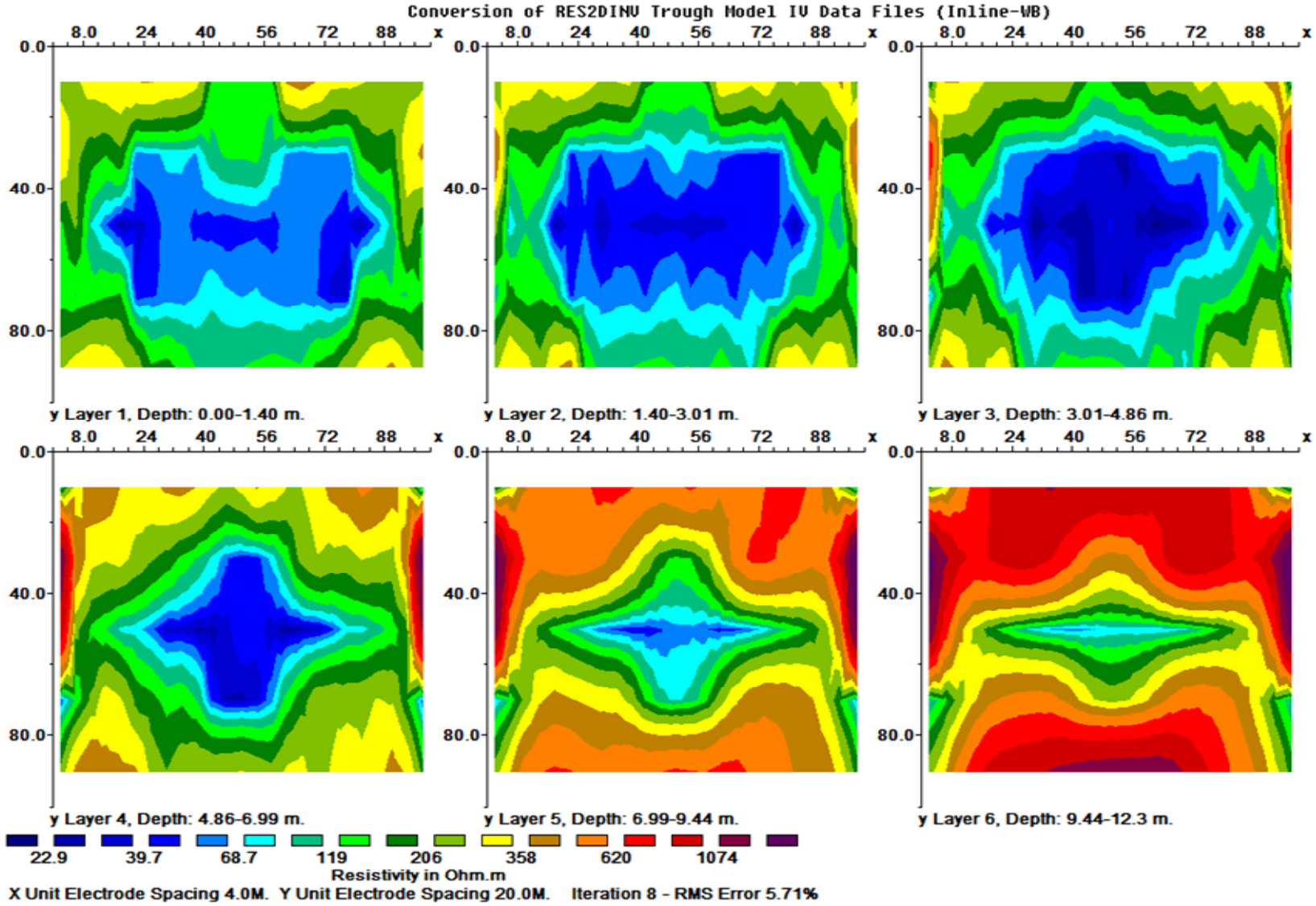

b(WB)

Figure 7. Horizontal depth slices of the inverse models of parallel 2D profiles for the trough model structure with a grid size of 26×6 and inter-line spacing of $5a$: (a) Wenner-alpha; and (b) Wenner-beta.

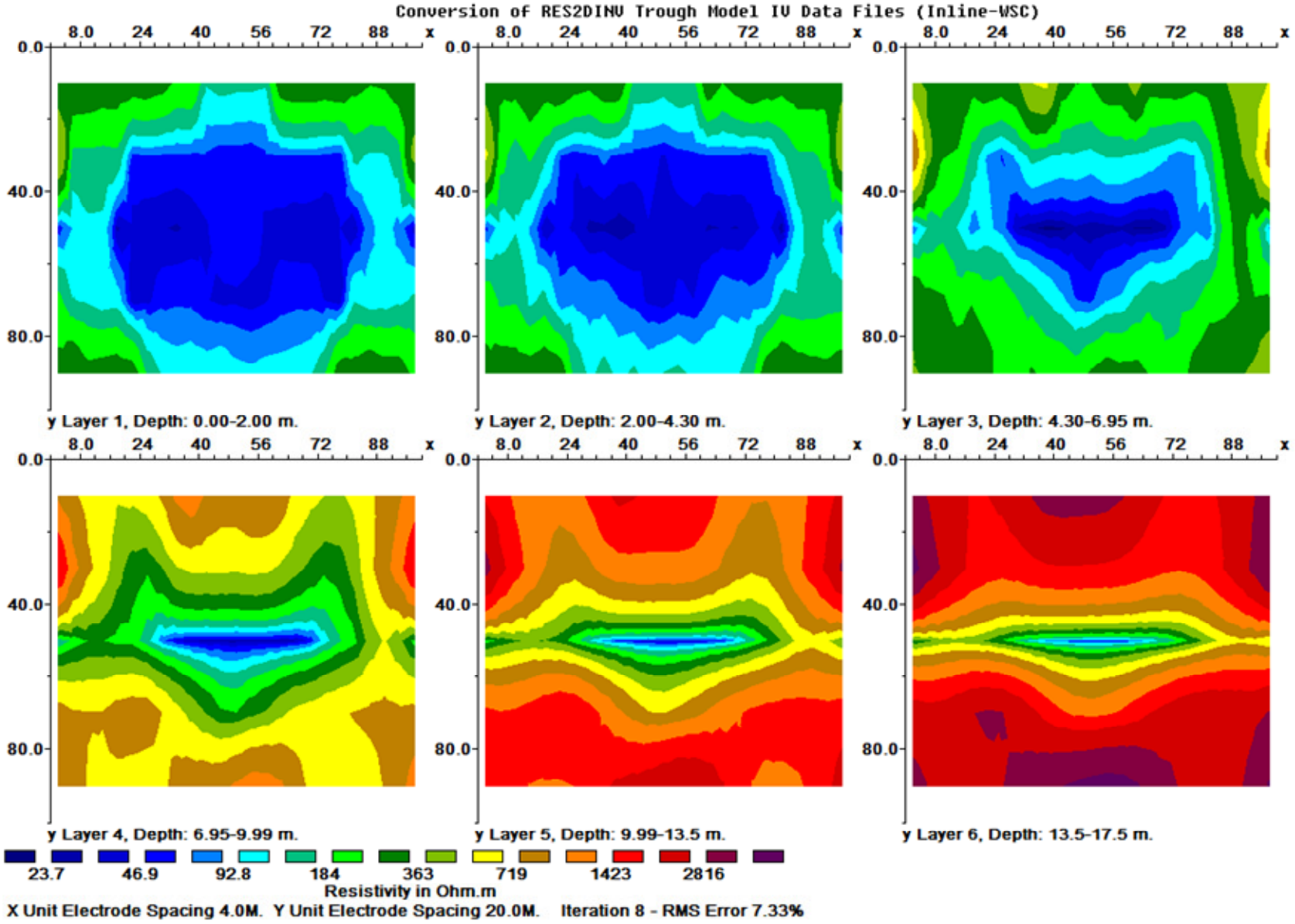
Conversion of RES2DINV Trough Model IV Data Files (Inline-WSC)
8.0 24 40 56 72 88 x
0.0
40.0
80.0
y Layer 1, Depth: 0.00-2.00 m.
y Layer 2, Depth: 2.00-4.30 m.
y Layer 3, Depth: 4.30-6.95 m.
y Layer 4, Depth: 6.95-9.99 m.
y Layer 5, Depth: 9.99-13.5 m.
y Layer 6, Depth: 13.5-17.5 m.
23.7 46.9 92.8 184 363 719 1423 2816
Resistivity in Ohm.m
X Unit Electrode Spacing 4.0M. Y Unit Electrode Spacing 20.0M. Iteration 8 - RMS Error 7.33%

a(WSC)

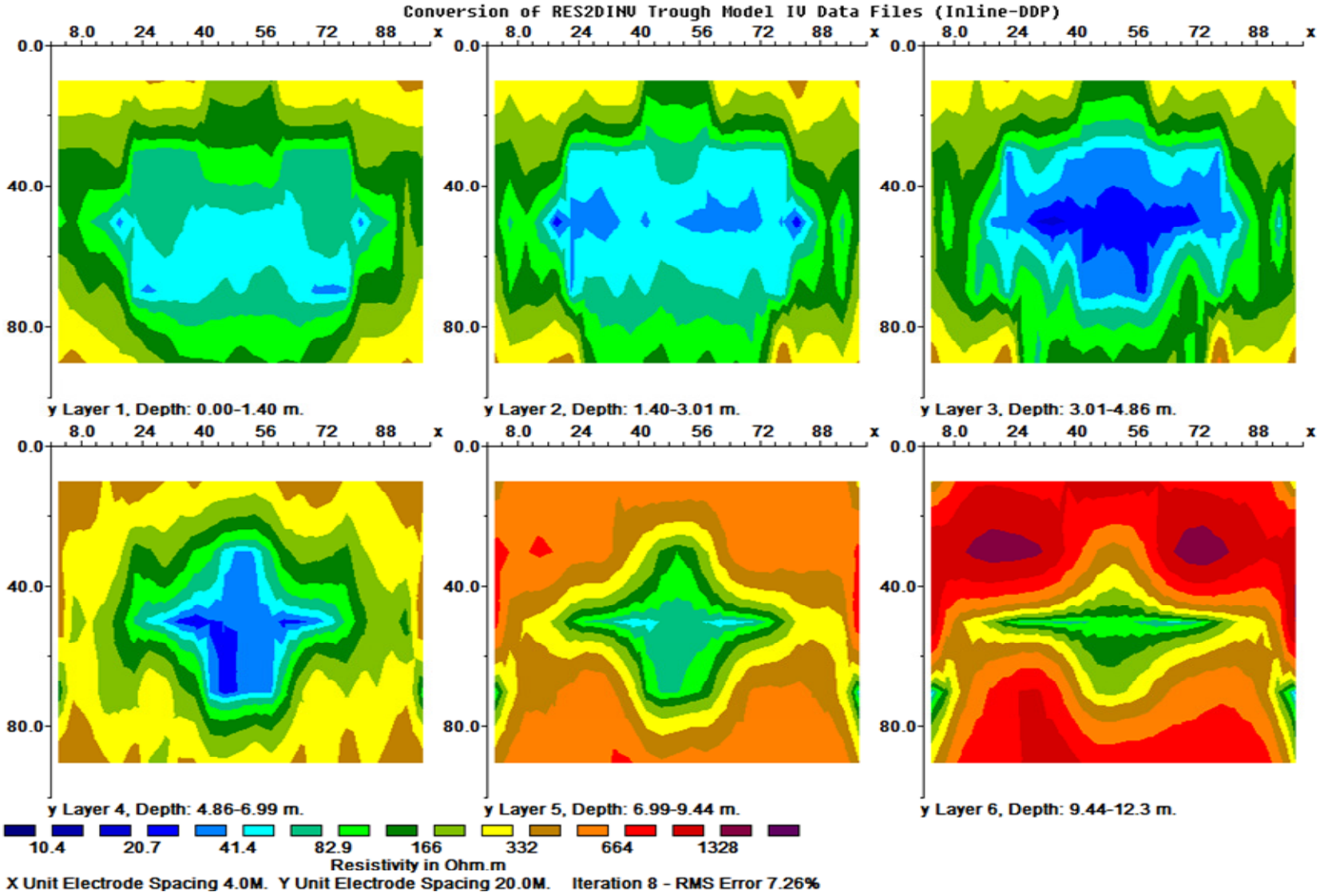

Figure 8. Horizontal depth slices of the inverse models of parallel 2D profiles for the trough model structure with a grid size of 26×6 and inter-line spacing of $5a$: (a) Wenner-Schlumberger; and (b) dipole-dipole.

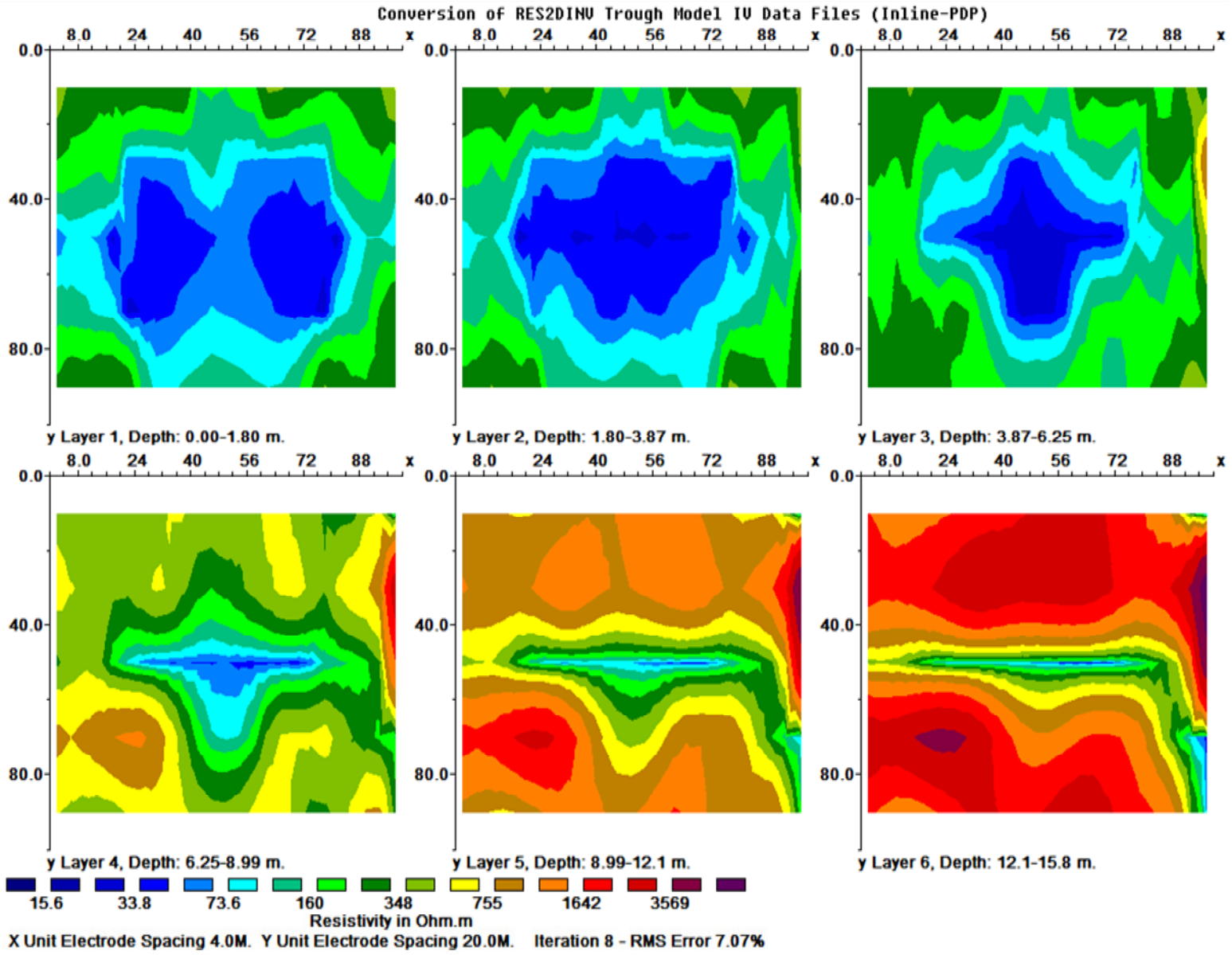
Conversion of RES2DINV Trough Model IV Data Files (Inline-PDP)
8.0 24 40 56 72 88 x
0.0
40.0
80.0
y Layer 1, Depth: 0.00-1.80 m.
y Layer 2, Depth: 1.80-3.87 m.
y Layer 3, Depth: 3.87-6.25 m.
y Layer 4, Depth: 6.25-8.99 m.
y Layer 5, Depth: 8.99-12.1 m.
y Layer 6, Depth: 12.1-15.8 m.
15.6 33.8 73.6 160 348 755 1642 3569
Resistivity in Ohm.m
X Unit Electrode Spacing 4.0M. Y Unit Electrode Spacing 20.0M. Iteration 8 - RMS Error 7.07%

a(PDP)

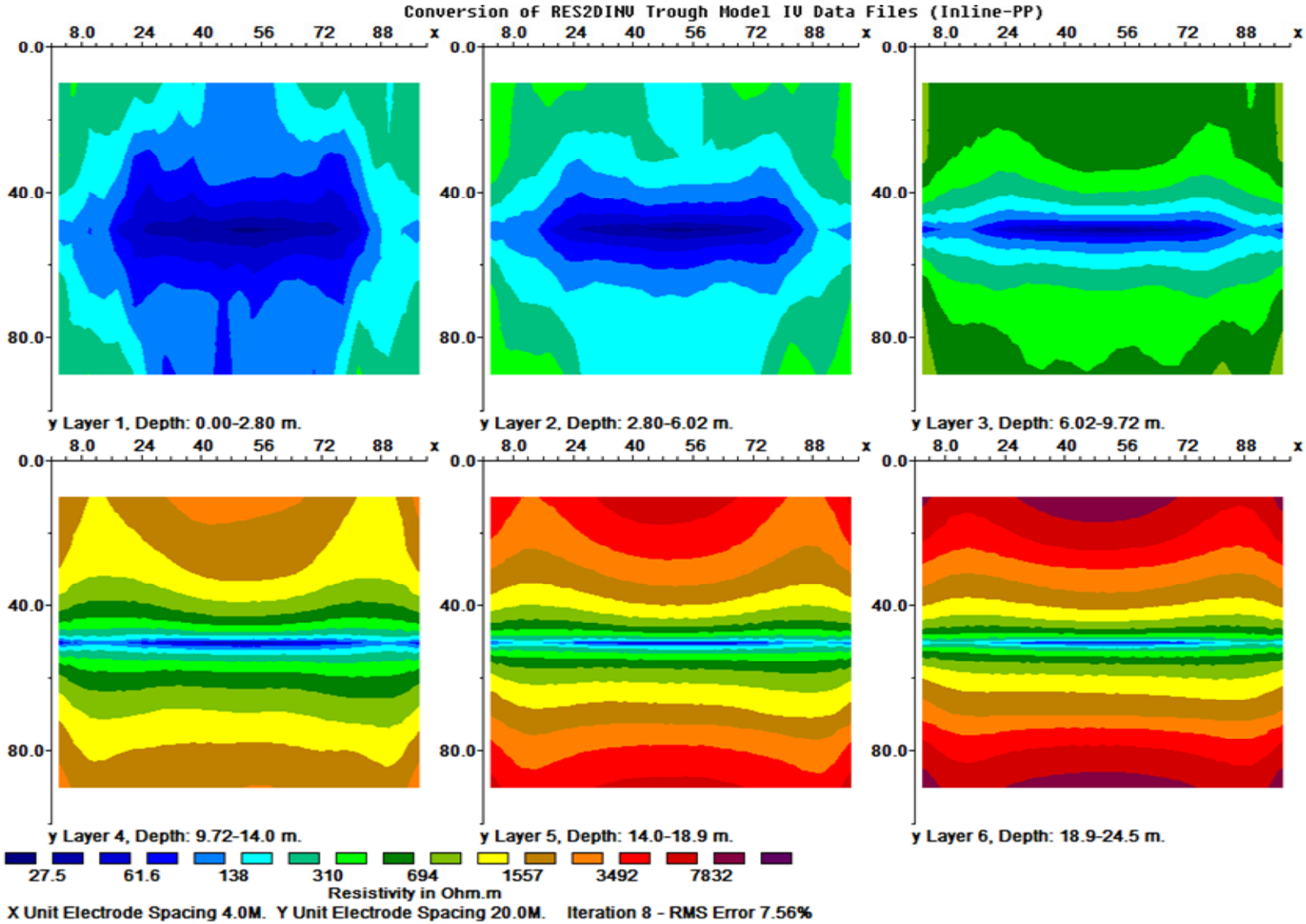

Figure 9. Horizontal depth slices of the inverse models of parallel 2D profiles for the horst model structure with a grid size of 21×6 and inter-line spacing of $4a$: (a) pole-dipole; and (b) pole-pole.

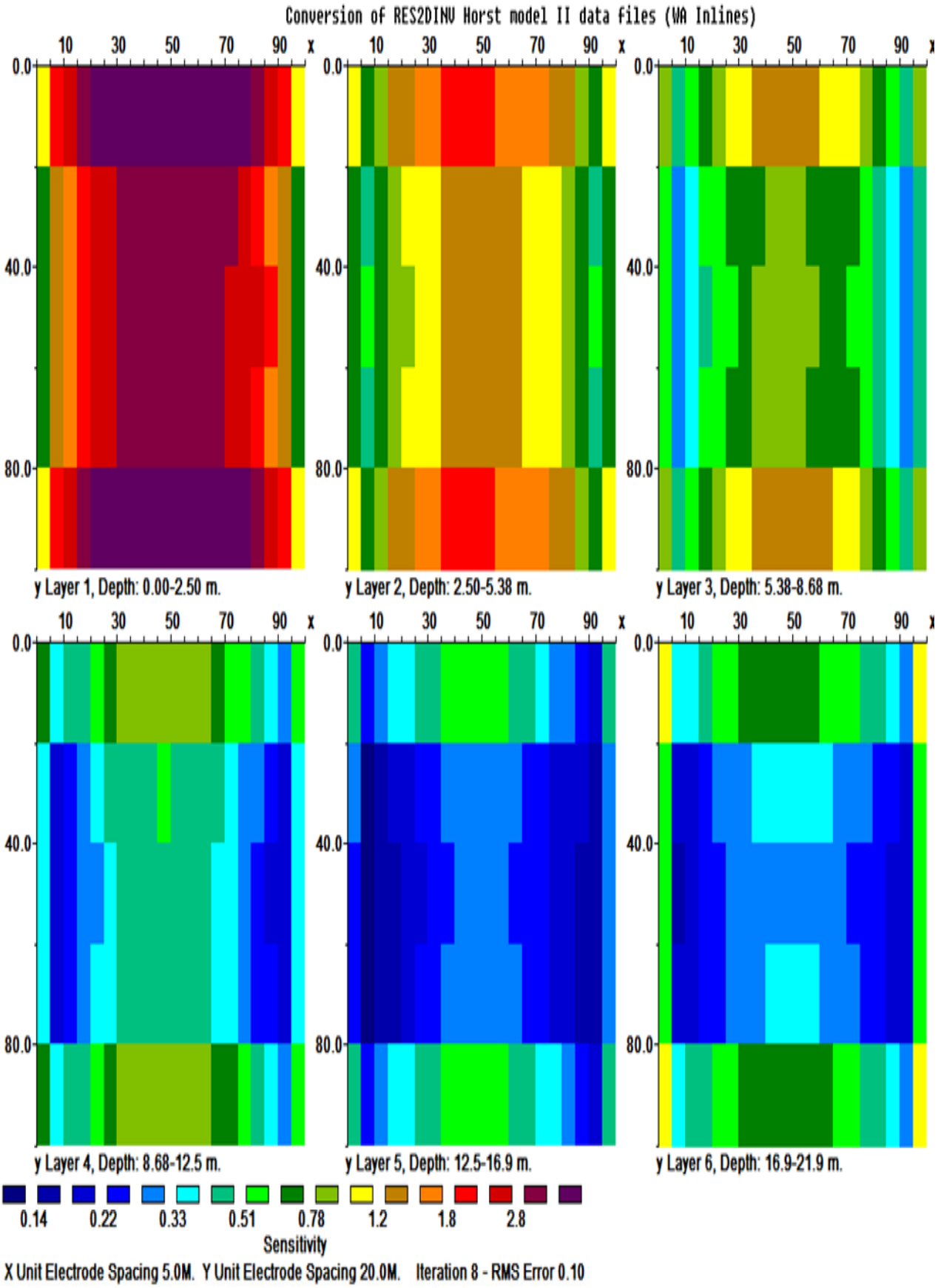
Conversion of RES2DINV Horst model II data files (WA Inlines)
10 30 50 70 90 x
0.0
40.0
80.0
y Layer 1, Depth: 0.00-2.50 m.
y Layer 2, Depth: 2.50-5.38 m.
y Layer 3, Depth: 5.38-8.68 m.
y Layer 4, Depth: 8.68-12.5 m.
y Layer 5, Depth: 12.5-16.9 m.
y Layer 6, Depth: 16.9-21.9 m.
0.14 0.22 0.33 0.51 0.78 1.2 1.8 2.8
Sensitivity
X Unit Electrode Spacing 5.0M. Y Unit Electrode Spacing 20.0M. Iteration 8 - RMS Error 0.10

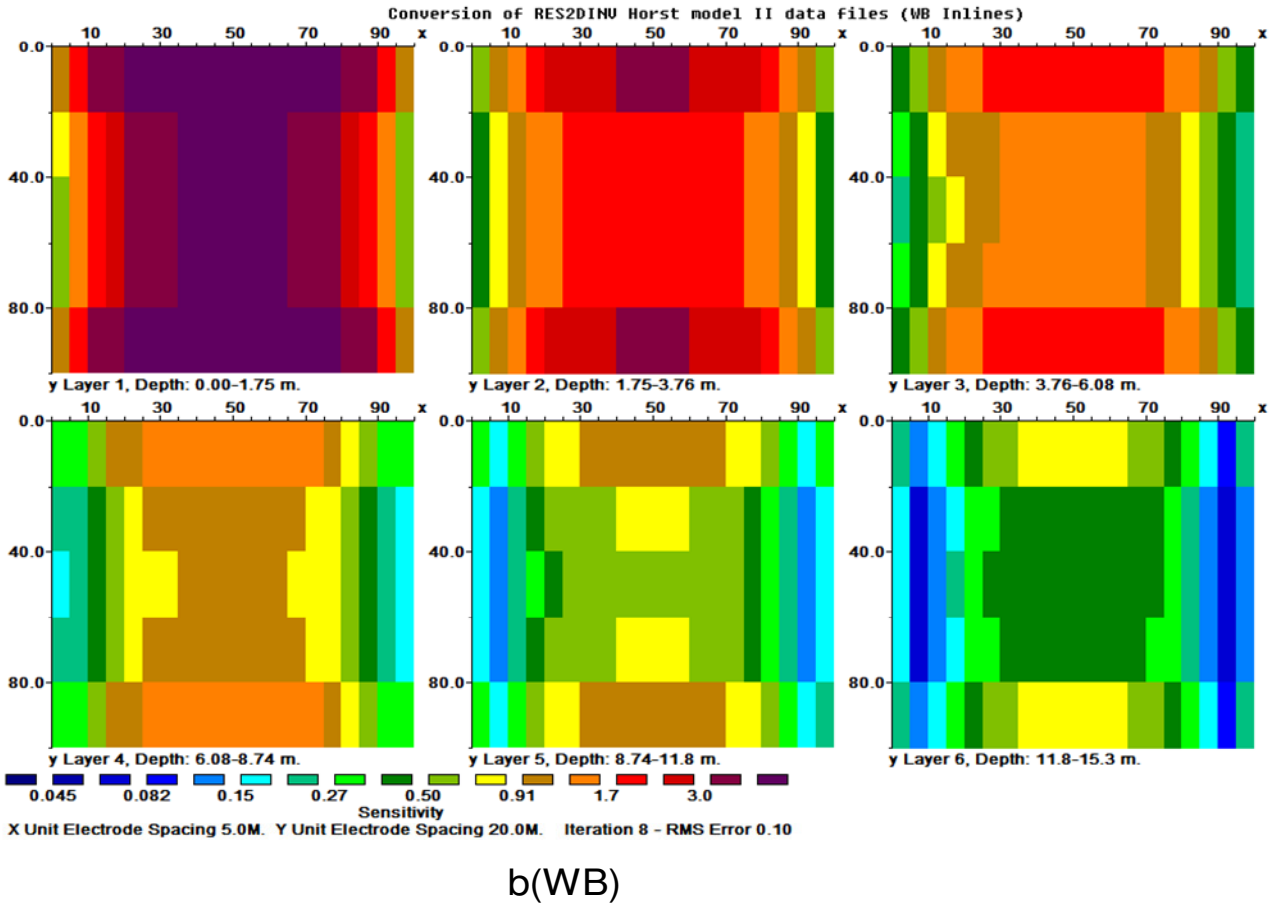

Figure 10. Horizontal depth slices of the sensitivity models of parallel 2D profiles for the horst model structure with a grid size of 21×6 and inter-line spacing of $4a$: (a) Wenner-alpha; and (b) Wenner-beta.

If sparse set of parallel 2D profiles are used for the 3D survey, the time required for the survey would be significantly reduced; but this is however at the expense of the resolution of the 3D inverse models. The set of parallel 2D profiles could results in small-scale near-surface spurious artefacts in the inverse resistivity models due to the projection of the anomalies located in the deeper parts of the models. However, such 3D inverse models could provide useful guide in the interpretation of 3D variation of the subsurface resistivity/conductivity as well as 3D subsurface features.

Thus, meaningful 3D information on the subsurface features can be extracted from the 3D inverse models.

However, grid orientation effect is observed in both structures investigated. The inverse models are observed to be oriented perpendicularly to the direction of the parallel 2D profiles. The grid orientation effect is independent of the subsurface features to be mapped. This is evident in the inversion images of the two models, horst and trough structure, presented in this study. The observed grid orientation effects could be misleading in the interpretation of subsurface features. The effect of grid orientation decreases with decreasing profiles inter-line spacing relative to the minimum electrode separation. Thus, the effect of grid orientation could be minimized or completely eliminated if closely spaced 2D profiles are used relative to the minimum electrode spacing. Also, the grid orientation effects could be minimized by using orthogonal 2D profiles to build the 3D data set without necessarily using the same minimum electrode separations and inter-line spacing in both x- and y-directions (Garibi and Bentley, 2005; Aizebeokhai et al., 2010).

The model sensitivities of the data set for each array were assessed (Figures 10 to 15). Wenner-beta and Wenner-Schlumberger arrays shows higher more uniform model sensitivities in the sensitivity maps. However, low model sensitivities are observed at the edges of the sensitivity maps. The model sensitivity of Wenner-alpha array decreases sharply with depth. The model sensitivities of dipole-dipole and pole-dipole arrays are moderate, though edge effects are also observed in the sensitivity maps of these arrays. In general, pole-pole array show the least model sensitivities in the inversion models; unrealistic edge effects are also observed in the sensitivity of the arrays.

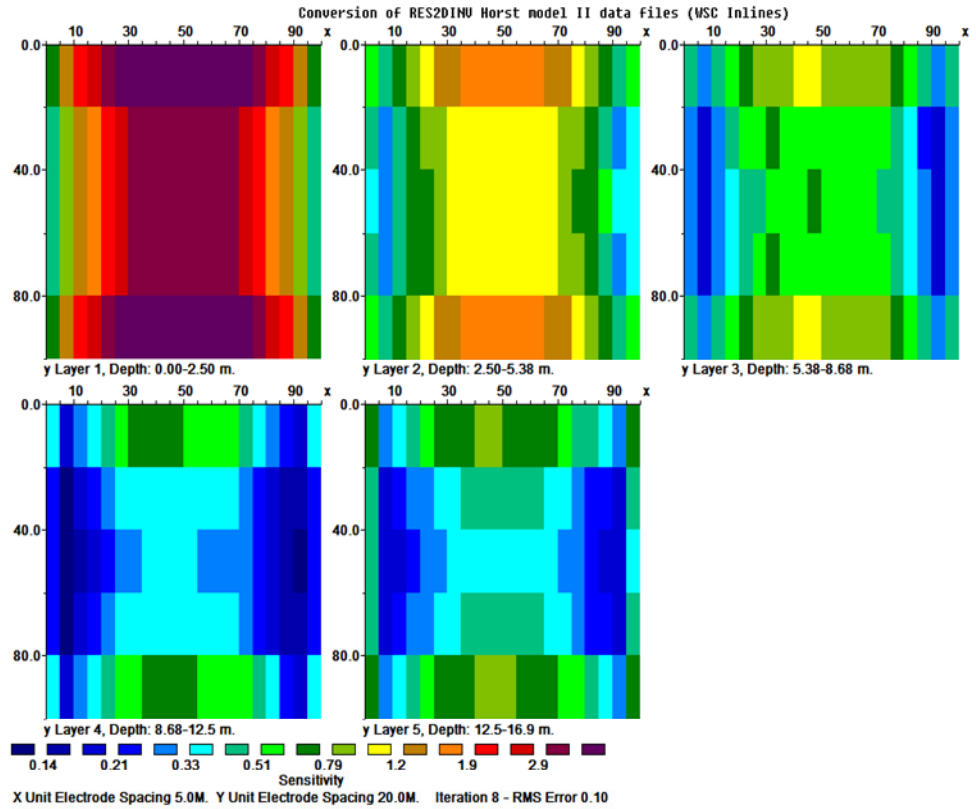

a(WSC)

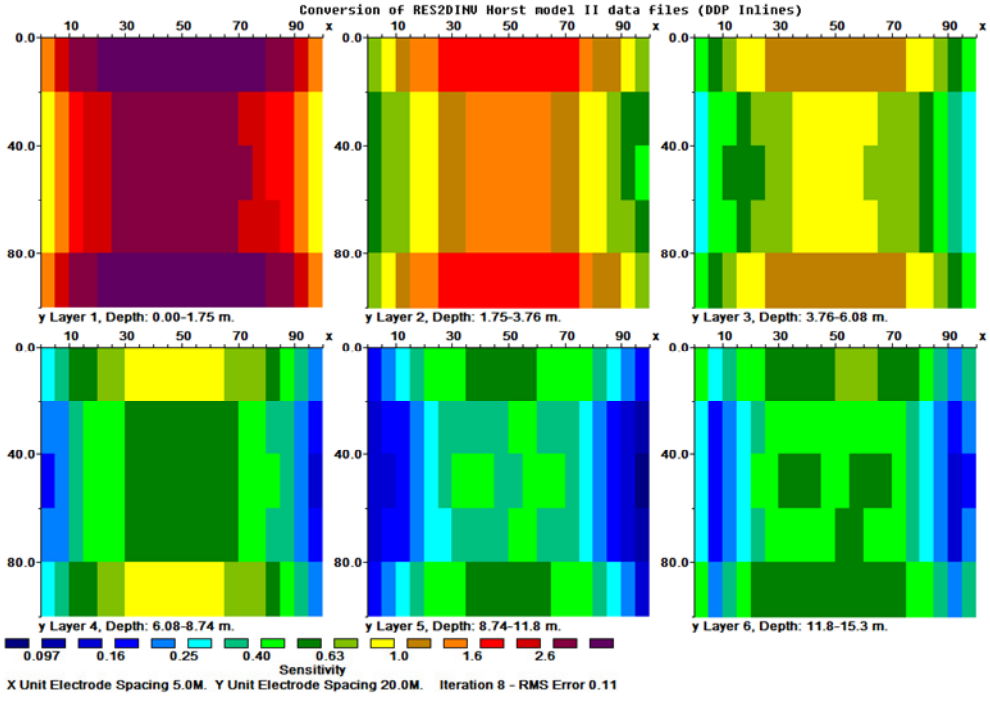

b(DDP)

Figure 11. Horizontal depth slices of the sensitivity models of parallel 2D profiles for the horst model structure with a grid size of 21×6 and inter-line spacing of $4a$: (a) Wenner-Schlumberger; and (b) dipole-dipole.

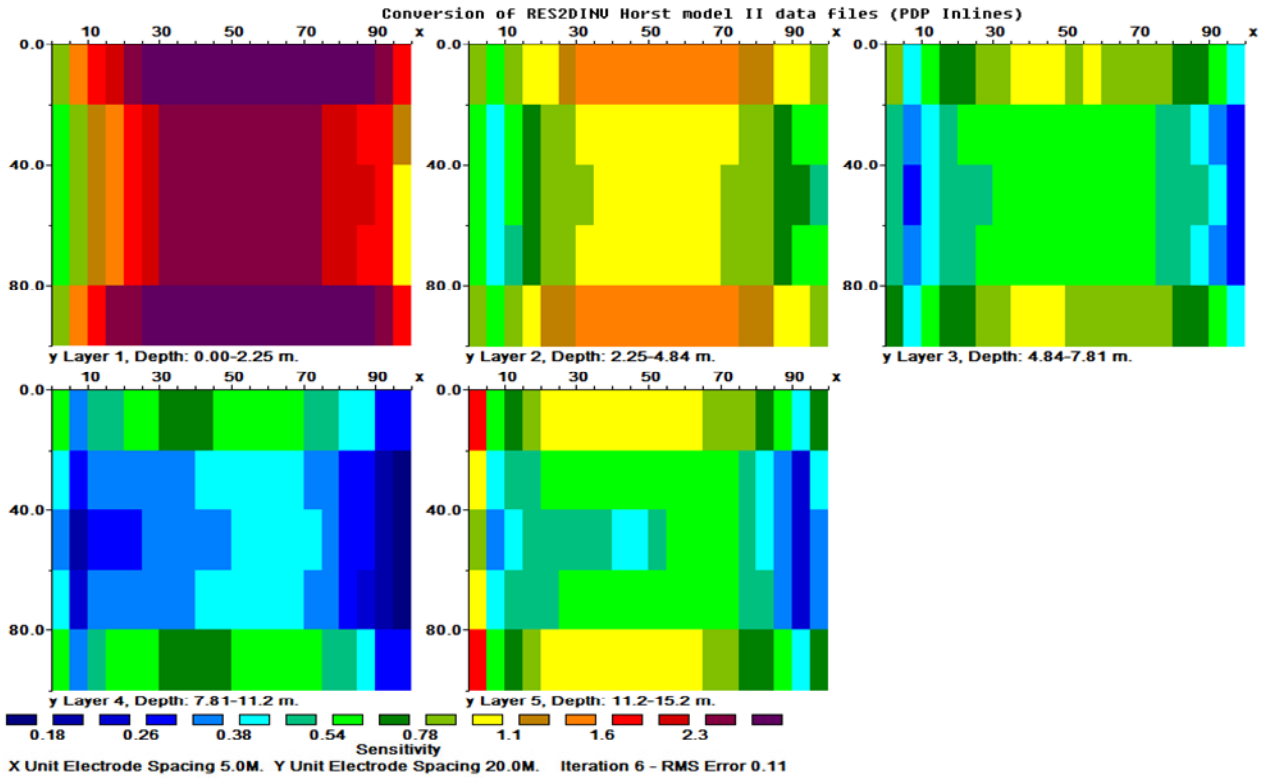

a(PDP)

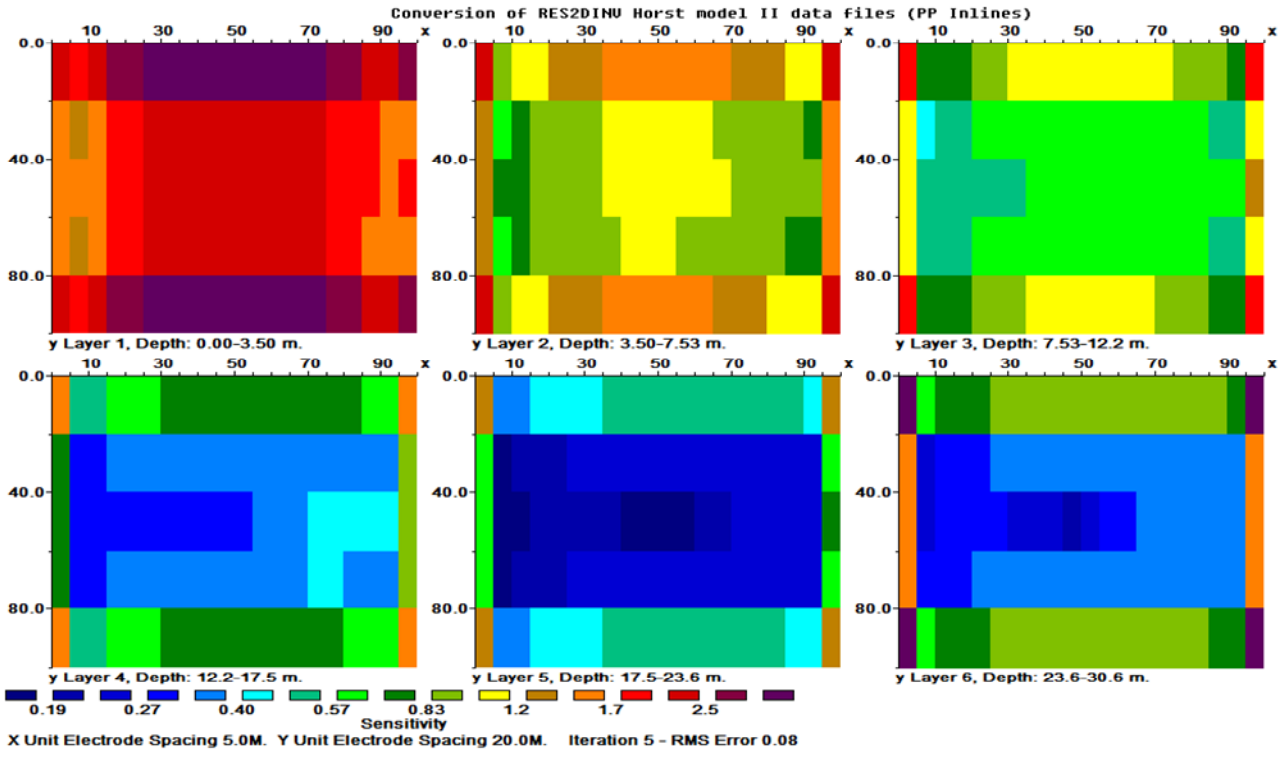

b(PP)

Figure 12. Horizontal depth slices of the sensitivity models of parallel 2D profiles for the horst model structure with a grid size of 21×6 and inter-line spacing of $4a$: (a) pole-dipole; and (b) pole-pole.

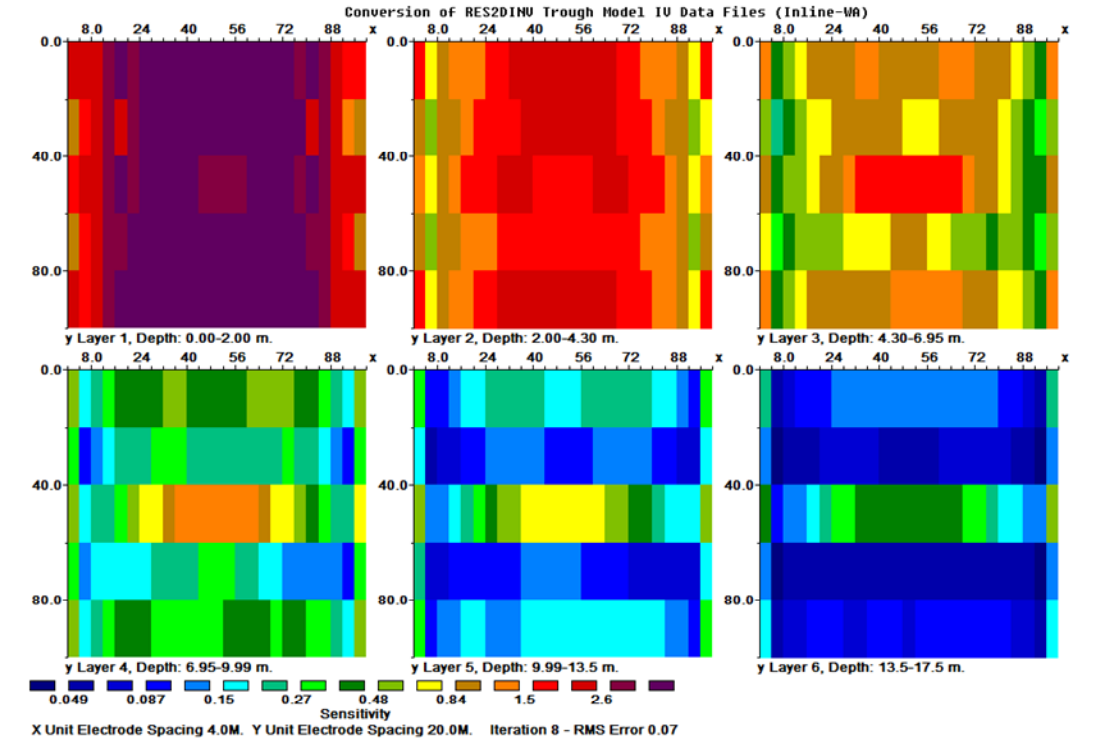

a(WA)

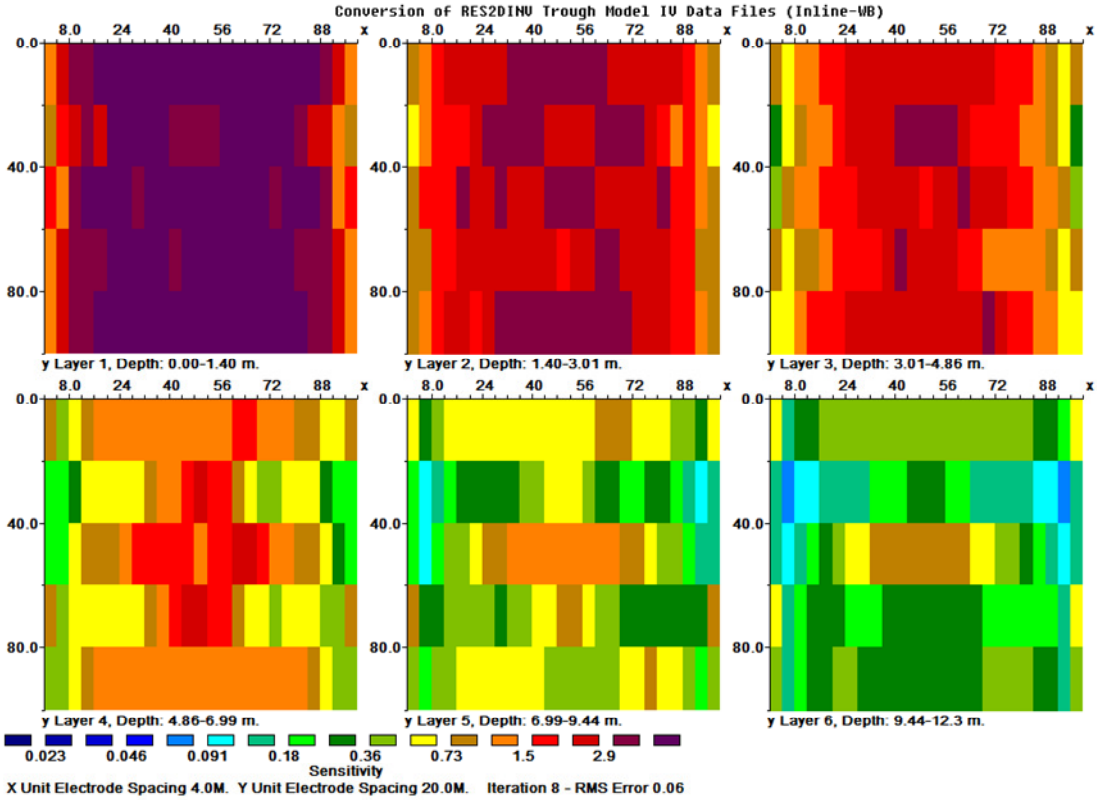

b(WB)

Figure 13. Horizontal depth slices of the sensitivity models of parallel 2D profiles for the trough model structure with a grid size of 21×6 and inter-line spacing of $4a$: (a) Wenner-alpha; and (b) Wenner-beta.

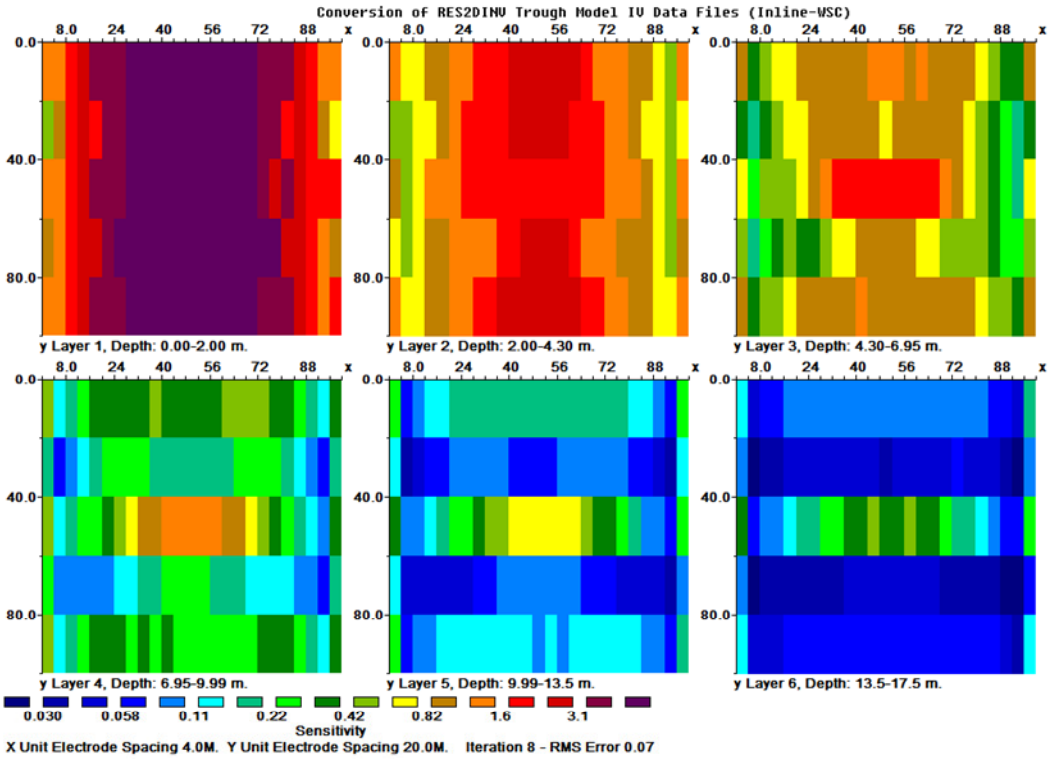

a(WSC)

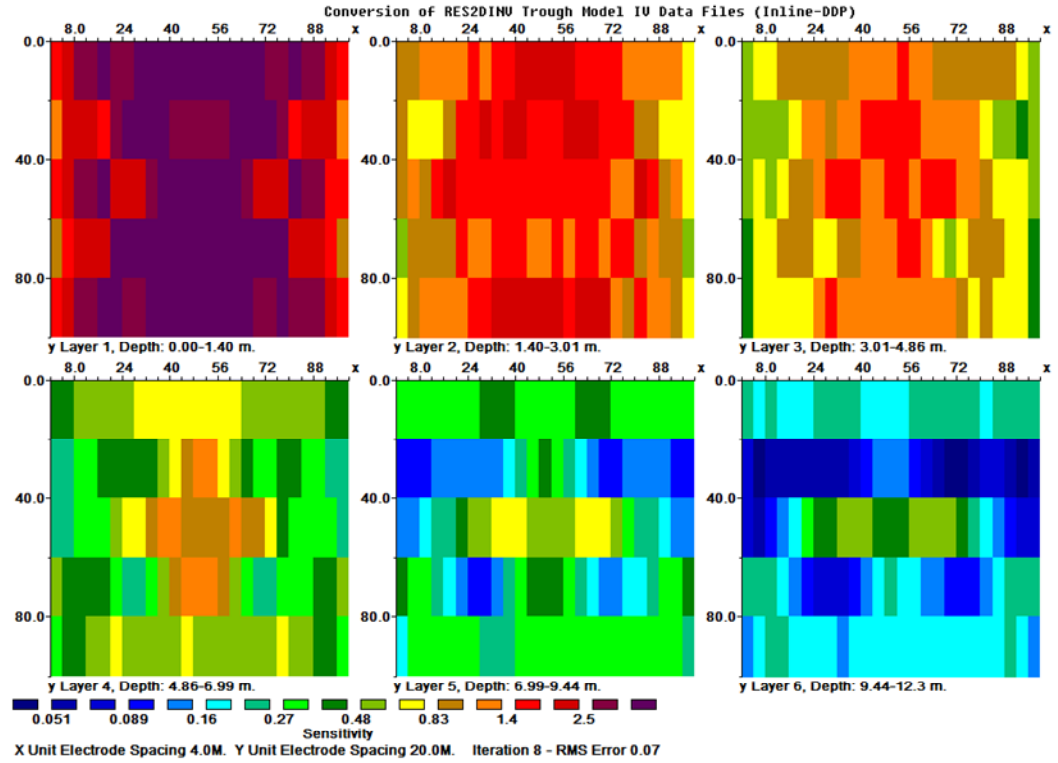

b(DDP)

Figure 14. Horizontal depth slices of the sensitivity models of parallel 2D profiles for the trough model structure with a grid size of 21×6 and inter-line spacing of $4a$: (a) Wenner-Schlumberger; and (b) dipole-dipole.

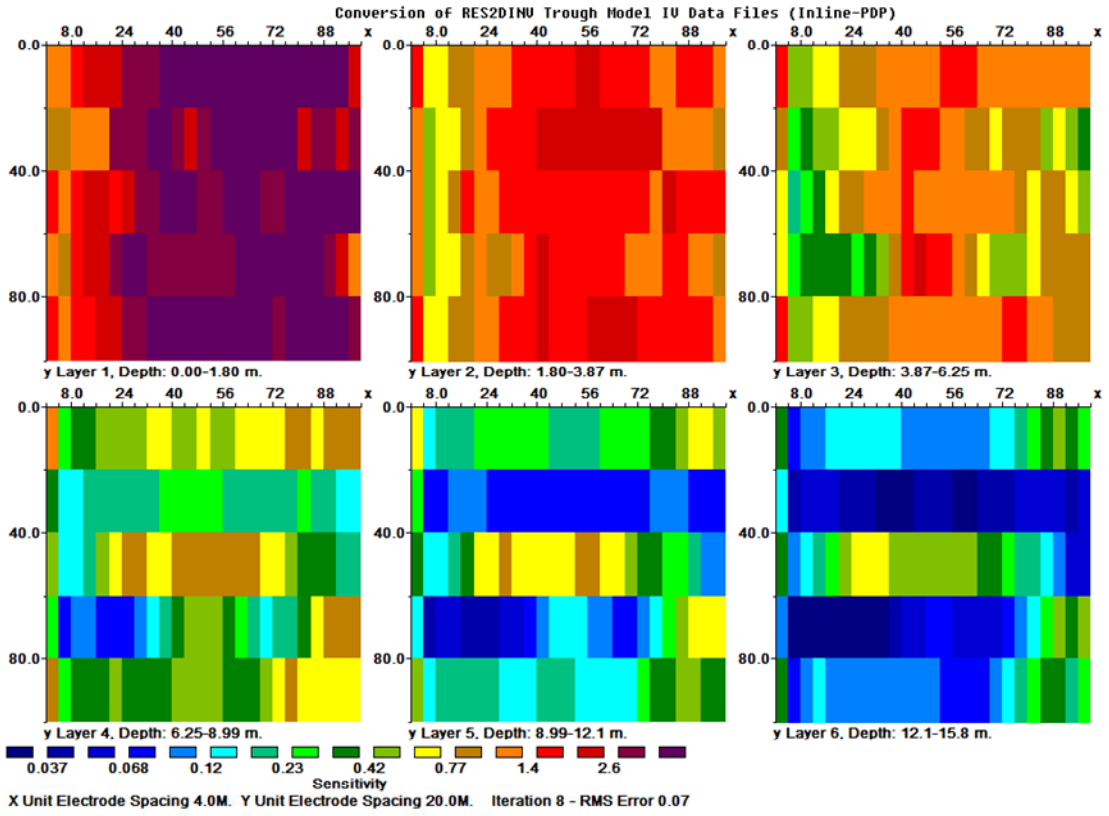

a(PDP)

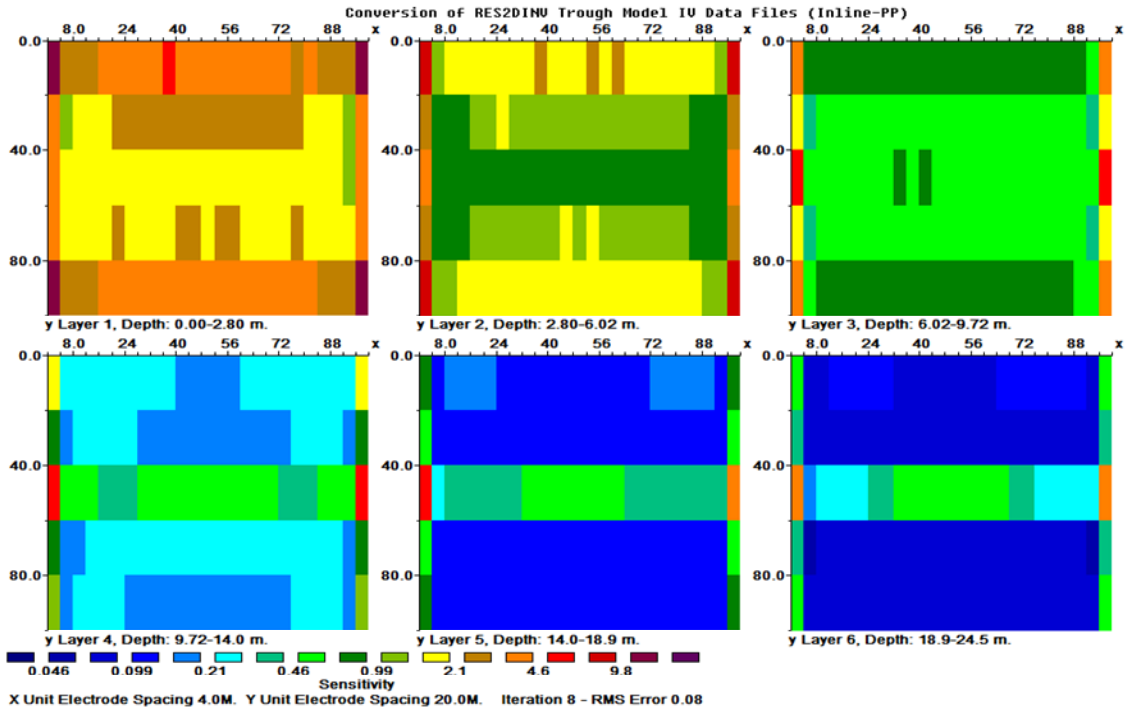

b(PP)

Figure 15. Horizontal depth slices of the sensitivity models of parallel 2D profiles for the trough model structure with a grid size of 21×6 and inter-line spacing of $4a$: (a) pole-dipole; and (b) pole-pole.

Conclusion

The use of parallel 2D profiles in generating 3D data set is a fast and cost effective technique of conducting 3D geoelectrical resistivity surveys. The inter-line spacing should not be greater than four times the minimum electrode separation for good quality and high resolution 3D inversion images. The resolution of the inversion images can be enhanced by using closing spaced 2D profiles or orthogonal 2D profiles. The model sensitivities of the inverse models indicate that Wenner-beta, Wenner-Schlumberger and dipole-dipole arrays are more sensitive to the 3D features, while pole-pole array is the least sensitivity array to the 3D features. The inverse models are, however, characterised with grid orientation effects which can be misleading in subsurface features interpretation. The grid orientation effect can be minimised by reducing the inter-line spacing relative to the minimum electrode separation or eliminated by collating orthogonal 2D profiles to 3D data set.

ACKNOWLEDGMENTS

The Third World Academy of Science (TWAS), Italy in collaboration with the Council of Scientific and Industrial Research (CSIR), India are gratefully acknowledged by the first author for providing the Fellowship for this study at the National Geophysical Research Institute (NGRI), Hyderabad, India.

REFERENCES

Aizebeokhai AP, Olayinka AI, Singh VS (2009). Numerical evaluation of 3D geoelectrical resistivity imaging for environmental and engineering investigations using orthogonal 2D profiles, SEG Exp. Abstracts, 28: 1440-1444.

Aizebeokhai AP, Olayinka AI, Singh VS (2010). Application of 2D and 3D geoelectrical resistivity imaging for engineering site investigation in a crystalline basement terrain, southwestern Nigeria. J. Environ. Earth Sci., 61(7): 1481-1492.

Amidu SA, Olayinka AI (2006). Environmental assessment of sewage disposal systems using 2D electrical resistivity imaging and geochemical analysis: A case study from Ibadan, Southwestern Nigeria. Environ. Eng. Geosci., 7(3): 261-272.

Bentley LR, Gharibi M (2004). Two- and three-dimensional electrical resistivity imaging at a heterogeneous site. Geophy, 69(3): 674-680.

Carruthers RM, Smith IF (1992). The use of ground electrical survey methods for sitting water supply boreholes in shallow crystalline basement terrain. In: Wright EP, Burgess, WG (Eds.), Hydrogeology of Crystalline basement Aquifers in Africa. Geol. Soc. Spec. Public, 66: 203-220.

Chambers JE, Ogilvy RD, Meldrum PI, Nissen J (1999). 3D electrical resistivity imaging of buried oil-tar contaminated waste deposits. Eur. J. Environ. Eng. Geophys., 4: 3-15.

Dahlin T, Loke MH (1998). Resolution of 2D Wenner resistivity imaging as assessed by numerical modelling. J. Appl. Geophy., 38(4): 237-248.

Dey A, Morrison HF (1979). Resistivity modelling for arbitrary shaped two-dimensional structures. Geophy. Prosp., 27: 1020-1036.

Gharibi M, Bentley LR (2005). Resolution of 3D electrical resistivity images from inversion of 2D orthogonal lines. J. Environ. Eng. Geophys., 10(4): 339-349.

Griffiths DH, Barker RD (1993). Two dimensional resistivity imaging and modeling in areas of complex geology. J. Appl. Geophys., 29: 211-226.

Hazell JRT, Cratchley CR, Jones CRC (1992). The hydrology of crystalline aquifers in northern Nigeria and geophysical techniques used in their exploration. In: Wright EP, Burgess WG (Eds.), Hydrogeology of Crystalline basement Aquifers in Africa. Geol. Soc. Spec. Publ., 66: 155-182.

Li Y, Oldenburg DW (1994). Inversion of 3D DC resistivity data using an approximate inverse mapping. Geophys. J. Int., 116: 527-537.

Loke MH, Barker RD (1996a). Practical techniques for 3D resistivity surveys and data inversion. Geophy. Prosp., 44: 499-524.

Loke MH, Barker RD (1996b). Rapid least-squares inversion of apparent resistivity pseudosections by a quasi-Newton method. Geophys. Prosp., 44: 131-152.

Ogilvy R, Meldrum P, Chambers J (1999). Imaging of industrial waste deposits and buried quarry geometry by 3D tomography. Eur. J. Environ. Eng. Geophys., 3: 103-113.

Olayinka AI, Yaramanci U (1999). Choice of the best model in 2-D geoelectrical imaging: case study from a waste dump site. Eur. J. Environ. Eng. Geophys., 3: 221-244.

Park S (1998). Fluid migration in the vadose zone from 3D inversion of resistivity monitoring data. Geophy. 63**:** 41-51.

Press WH, Teukolsky SA, Vetterling WT, Flannery BP (1996). Numerical recipes in Fortran 77: The Art of Scientific Computing, 2nd edn., Cambridge University Press.

White RMS, Collins S, Denne R, Hee R, Brown P (2001). A new survey design for 3D IP modelling at Copper hill. Expl. Geophys., 32: 152-155.